JOHANNES KEPLER
UNIVERSITY LINZ

MODELING AND SIMULATION OF MIXING IN SINGLE-SCREW EXTRUDERS – DESIGN AND OPTIMIZATION

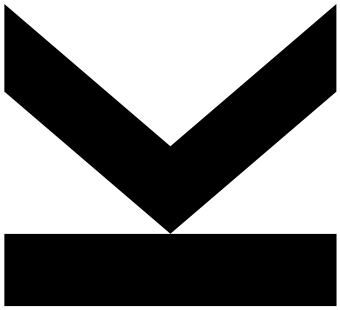

Final Report – Marshall Plan Scholarship

Submitted by:
DI Christian Marschik, BSc
Researcher
Institute of Polymer Extrusion and Compounding
Johannes Kepler University Linz

JOHANNES KEPLER
UNIVERSITY LINZ
Altenberger Str. 69
4040 Linz, Austria
www.jku.at
DVR 0093696

Table of Contents

1. Introduction

Single-screw extruders are the most important type of machinery in the polymer-processing industry. Due to their simple design and great versatility, they are used in many polymer-shaping processes, producing a wide variety of plastic products such as pipes, films, profiles, fibers, cables, and sheets. A significant proportion of polymers passes through a single-screw extruder at least once after manufacture. The prominent position of the screw-barrel configuration in the polymer-processing field is based on its continuous development over the past few decades. This technical progress has gone hand in hand with extensive theoretical and experimental research. Thorough reviews of the process can be found in [1-4]. To meet the ever-increasing demands on the machinery, the process requires further optimization and thus a deeper understanding of the transport mechanisms governing physical operation.

1.1. The Plasticating Single-Screw Extruder

Single-screw extruders come in various designs. The research reported here focuses on plasticating single-screw extruders, as illustrated schematically in Fig. 1.

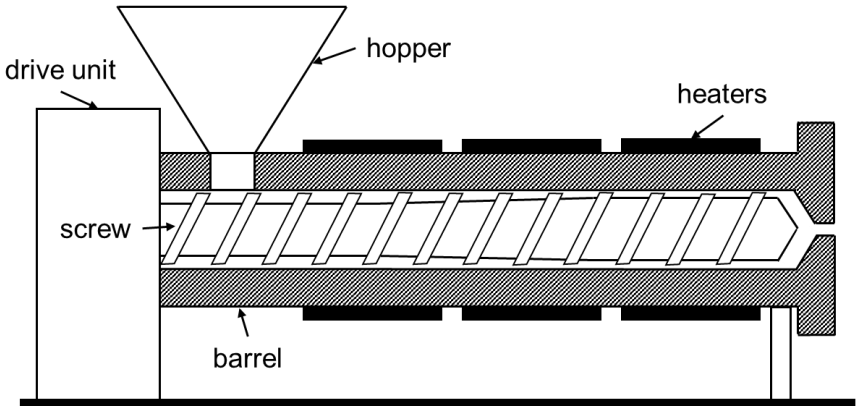

Figure 1: Schematic of a plasticating single-screw extruder.

The plasticating extrusion process starts with the feedstock material entering the extruder barrel. The solid feed, typically in the form of pellets or powders, is usually a composition of polymers, fillers and additives. As the feed falls down into the screw channel, frictional forces caused by the relative movement of the rotating screw and the stationary barrel act on the solids, thus transporting the material forward. This functional screw part, which is concerned with transport and compaction of the solids, is commonly referred to as solids-conveying zone. Two sources supply energy to heat and melt the polymer: The main energy input comes from the rotating shaft, which introduces mechanical energy to the system that is converted into thermal energy due to viscous dissipation. In addition, barrel heaters located at the outside of the barrel provide thermal energy via conductive heating. As a result of internal and external heating, the temperature of the polymer increases and melting is initiated. In the melting zone, the polymer is converted from solid to liquid. The solid fraction decreases continuously while the melt fraction increases. Melting has completed once the solid fraction has been converted completely into melt. The molten polymer is then conveyed through the metering zone or melt-conveying zone. In this section, the melt is pumped and pressurized for downstream operation.

1.2. Mixing in Single-Screw Extrusion

A key step in all extrusion operations is mixing. The primary objective of single-screw extruders is to provide excellent melt homogeneity at high output rates and proper discharge temperatures. Poorly mixed polymer melts are likely to cause defects in the parts produced, increasing both rejection rates and production costs. In general, single-screw extruders are employed for several mixing applications (as listed, e.g., in [5]). The general aim of mixing is to reduce the non-uniformity of a system comprised of two or more substances [6]. A highly critical parameter that is not strictly related to the presence of multiple components but also depends strongly on the mixing performance of the machine is the thermal homogeneity of the discharge. The flow field in the screw channel is often subject to high deformation rates, which causes excessive shearing and stretching of the polymer chains. Due to inner friction between adjacent fluid elements, mechanical energy is transformed into heat, which leads to an uneven increase in melt temperature. Mitigating temperature gradients in the discharge is extremely important for eliminating surface defects, reducing shrinkage and warping, and thus maintaining high product quality.

In plasticating single-screw extrusion, mixing takes place at several stages. With the exception of the solids-conveying zone, where no mixing occurs, the mixing process extends from the melting zone to the end of the extruder. Pronounced mixing takes place first during melting of the solids [3]. Several high-performance screw designs have been developed that promote mixing. The main goal of these advanced screw concepts is to accelerate the melting process. Since mixing requires the polymer to be in the molten state, the sooner melting is completed, the higher the probability of achieving perfect mixing. The mixing process continues as the polymer melt is pumped and pressurized in the metering zone. Mixing in single-screw extruders is generally subject to significant non-uniformity. To finish the mixing process, many processors employ mixing elements downstream of the melting zone to homogenize the polymer melt further and disperse solid agglomerates. The number of mixing elements applied in industry is large and can be classified into four categories: (i) distributive, (ii) dispersive, (iii) static, and (iv) dynamic mixers.

1.3. Numerical Analyses of Mixing in Extrusion

Various numerical studies have investigated mixing in extruders by means of three-dimensional non-Newtonian flow analyses. Yang and Manas-Zloczower [7] as well as Cheng and Manas-Zloczower [8] were among the first to carry out three-dimensional finite-element simulations of the kneading disc region in a co-rotating twin-screw extruder. To increase the general understanding of mixing in intermeshing twin-screw extruders, several researchers have formulated their own finite-element models. Yoshinaga et al. [9], Ishikawa et al. [10,11], and Bravo [12] investigated the effect of screw configuration and processing conditions on the flow and mixing behavior in the kneading block section. Further, Ishikawa et al. [13] examined the influence of the tip-clearance on mixing performance.

These numerical studies considered transient flow boundary conditions. When simulating a sequence of instantaneous positions of the geometry, interpolation between the solutions of each snapshot yields the unsteady flow field. This modeling approach, however, involves significant effort in terms of meshing, since each individual flow configuration needs its own mesh to be defined. Moreover, it requires remeshing of the flow domain between the time steps in order to obtain time-dependent variables. Rios et al. [14] used the boundary element method to avoid remeshing algorithms. Since their technique was unable to capture the effects of non-linear flow behavior of the polymer melt, the authors used an oversimplified Newtonian model to describe the rheological nature

of the fluid. To combine the simplicity of mesh generation with the ability to deal with non-linear material characteristics, Avalosse and Rubin [15] presented the mesh superposition technique. This constrained finite-element method applies a penalty formulation to incorporate the velocity of the rotating screws into the mathematical formulation. Various studies have validated this technique against classical numerical simulations for both isothermal and non-isothermal flow conditions [15-17]. An alternative approach from the class of fictitious domain methods was proposed by Bertrand et al. [18]. Here, the motion of the moving parts is captured by means of Langrange multipliers.

Most reports on flow simulations have concentrated on mixing in twin-screw extrusion, whereas single-screw extruders have received comparatively less attention. Numerical analyses of mixing in single-screw extrusion have been restricted mainly to mixing heads. These devices are usually located downstream of the melting zone and complete the mixing process. Using the flow analysis network method, Wang and Tsay [19] examined non-Newtonian flows in both distributive and dispersive mixing devices. Kubik et al. [20] and Sun et al. [21] applied the finite-element method to investigate dispersive mixing in Maddock mixers. Further, Rios et al. [22] presented a parametric design study in which the mixing efficiencies of several configurations of a rhomboidal mixing screw were compared using the boundary element method. In a similar manner, Rauwendaal et al. [23] analyzed a dispersive mixing technology referred to as CRD mixer.

1.4. Research Objective

The research reported here used three-dimensional non-Newtonian flow simulations to investigate the pumping and mixing capability of block-head mixers. Block-head mixers are basically distributive mixing screws that are widely used to homogenize the polymer melt and eliminate thermal gradients. The polymer-processing industry employs a variety of block-head mixers, with little consensus on design and distribution of screw flights and mixing blocks. The present analysis addresses this issue based on a computational design study in which the influence of three geometrical parameters was examined: (i) the number of flights at a mixing block, (ii) the number of blocks along the screw, and (iii) the stagger angle between the blocks. To examine the flow behavior of the mixing screws, the pressure consumption and energy dissipation is evaluated. Distributive mixing is analyzed using residence time distribution functions, kinematic stretching parameters, and the scale of segregation. Dispersive mixing is assessed by means of the mixing index and the shear stress. The results of this design study increase the understanding of block-head mixers and contribute to the design and optimization of such geometries. The findings can further be applied to mixing screws of similar geometry, including pin-type and knob mixers.

2. Theoretical Background

Due to the high viscosity of polymer melts, mixing in single-screw extruders is governed by laminar flow, and neither turbulence nor molecular diffusion contributes measurably to the mixing performance. In general, mixing in extrusion processes can be classified into two categories: (i) distributive and (ii) dispersive mixing. The basic concepts of these mechanisms are shown in Fig. 2.

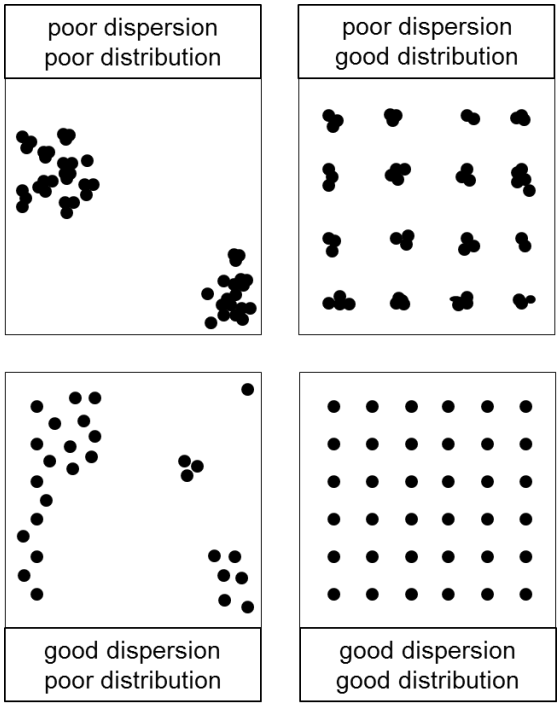

Figure 2: Basic concepts of distributive and dispersive mixing.

2.1. Distributive Mixing

Distributive mixing is required to achieve a uniform spatial distribution of the minor component within the major phase. By distributing the minor component throughout the flow domain, this type of mixing increases the homogeneity of the discharge. The process involves repeated rearrangement of the minor phase, which is achieved by multiple splitting, reorientation, and recombination of the flow. A critical parameter in distributive mixing is the total strain imposed on the fluid by either shearing or stretching, which causes the components to deform and the interfacial area to increase. The total strain to which the viscous polymer melt is exposed is limited by the rate of deformation and time. These properties change with the position in the screw channel, and consequently each fluid element exiting the process has a different flow and mixing history. Danckwerts [24] was the first to consider the residence-time distribution of fluid elements in continuous flow systems. He expressed the total fraction of exiting flow rate within a certain time period in the form of a cumulative residence time distribution function (CRTD):

$$F_{\mathrm{rt}}(t) = \int_{t_0}^{t} f_{\mathrm{rt}}(t)\,\mathrm{d}t\,, \tag{1}$$

where $f_{rt}(t)$ is the external residence time distribution function (RTD) and t_0 the minimum residence time. In a similar manner, Lidor and Tadmor [25] proposed the use of strain distribution functions to

express the non-uniformity in strain history. In this case, the total fraction of exiting flow rate that has experienced a certain range of strain values is obtained from:

$$F_s(\gamma) = \int_{\gamma_0}^{\gamma} f_s(\gamma)\,\mathrm{d}\gamma\,, \tag{2}$$

where $f_s(\gamma)$ is the strain distribution function (SDF) and γ_0 the minimum strain.

2.1.1. Characterization of Distributive Mixing

Various measures for quantifying distributive mixing can be found in the literature. One of the first parameters was presented by Danckwerts [26]: He investigated the homogenization process of a concentration field in a binary mixture and described the average striation thickness of the segregated regions using the scale of segregation:

$$s = \int_0^{\zeta} R(|r|)\,\mathrm{d}|r|\,. \tag{3}$$

To achieve perfect mixing, the concentrations of each fluid must disperse uniformly throughout the flow domain to produce a mixture of even concentration. The coefficient of correlation R(r) defines the degree of correlation between the concentrations and describes the probability of finding a pair of points, separated by a defined distance, at the same concentration:

$$R(r) = \frac{\sum_{i=1}^{M}\left(c_i' - c_{\mathrm{mean}}\right)\left(c_i'' - c_{\mathrm{mean}}\right)}{M\sigma_s^{\,2}}\,, \tag{4}$$

where $\overline{c}$ is the mean concentration of the mixture, M is the total number of pairs of points randomly placed in the mixture, and c_i' and c_i'' are the concentrations of the i^{th} pair of points. Two boundaries are defined: R(r) = 1 if the concentration is equal at both points in each pair, and R(r) = 0 if one point is pure major and the other pure minor. The sample variance results from:

$$\sigma_s^{\,2} = \frac{\sum_{i=1}^{2M}\left(c_i' - c_{\mathrm{mean}}\right)^2}{2M-1}\,. \tag{5}$$

Given the limits R(0) = 1 and R(ζ) = 0, the scale of segregation is the integral of the coefficient of correlation over the distance between the points. Distributive mixing improves as the scale of segregation decreases, as shown in Fig. 3.

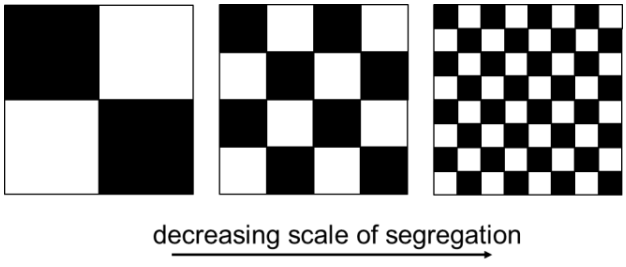

Figure 3: Scale of segregation.

Ottino [27] presented a kinematic approach based on continuum mechanics that tracks the amount of local deformation imposed on infinitesimal surface elements during the flow through a mixing zone.

Figure 4: Deformation of infinitesimal surfaces.

He introduced a kinematic parameter referred to as *local area stretch* that relates the magnitude of a deformed surface to its initial magnitude [28]:

$$\eta_m = \frac{|\mathrm{d}\boldsymbol{a}|}{|\mathrm{d}\boldsymbol{A}|}\,. \tag{6}$$

Good mixing is characterized by high values of the local area stretch. To describe the stretching rate of the infinitesimal surfaces being deformed, he additionally defined the *area stretching efficiency* as the fraction of total mechanical dissipation used to stretch the surface elements:

$$e_\eta = \frac{\mathrm{D}\ln(\eta_m)/\mathrm{D}t}{(\boldsymbol{D}:\boldsymbol{D})^{1/2}}\,. \tag{7}$$

A negative parameter value indicates a shrinking surface and a stretching volume in the normal direction [29], as shown in Fig. 4. The time-averaged area stretching efficiency was also defined as:

$$\langle e_\eta \rangle = \frac{1}{t}\int_0^t e_\eta \,\mathrm{d}t\,. \tag{8}$$

2.2. Dispersive Mixing

Dispersive mixing is required to reduce the size of a cohesive minor component, such as solid agglomerates, in a multiphase system. The cohesive strength of such clusters is due to London–van-der-Waals attraction forces. To separate cohesive particle clusters, the flow field must impose sufficiently high stresses that break up the agglomerates. In contrast to distributive mixing, which depends mainly on strain, dispersive mixing is governed by stresses acting on the components. Dispersive mixing plays a key role in the manufacture of compounds, which is usually performed using co-rotating twin-screw extruders. Although demand for single-screw extruders in compounding is increasing, these are generally unable to mix additives with polymers because they cannot perform the dispersive mixing required.

Dispersive mixing in single-screw extruders is required to disperse solid fragments entrapped in the polymer melt. This is particularly important in processes with increased melting lengths (e.g., high-speed extrusion processes), in which dispersive mixing completes the melting step. To impose large stresses on the solid components, mixing sections are typically designed with narrow flow channels, creating flow fields with high deformation rates. The conditions under which dispersive mixing takes place were first described by Bolen and Colwell [30]. They assumed that agglomerates break up when

the disruptive stresses acting on the solids as a result of viscous drag exceed a certain threshold value. Bird et al. [31] and Tadmor [32] refined the analysis of agglomerate rupture by calculating the maximum forces acting on an agglomerate, represented as a rigid dumbbell, for two types of flow: (i) a steady shear flow and (ii) a steady elongational flow. Assuming a Newtonian fluid, it was found that the maximum force in elongational flow is twice as high as in simple shear flow at the same rate of deformation and viscosity. Rauwendaal [4] concluded that, since the elongational viscosity of polymer melts is at least three times greater than the shear viscosity, the hydrodynamic forces generated in elongational flows are higher, and hence dispersive mixing is more efficient. Assuming the distance between both spheres of the dumbbell to be zero (see Fig 5), the separating forces are obtained from:

$$F_{\max,s} = 3\pi\tau_s r_1 r_2 , \tag{9}$$

$$F_{\max,e} = 6\pi\tau_e r_1 r_2 , \tag{10}$$

where τ_s and τ_e are the shear and elongational stresses, respectively, and r_1 and r_2 are the radii of the spheres. Manas-Zloczower and Fete [33,34] provided an extension of the model for other linear flow fields.

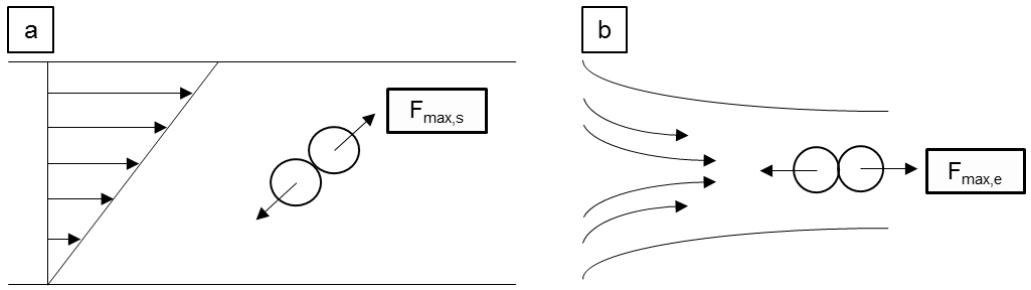

Figure 5: Maximum separating force between two spheres of radius r_1 and r_2 in a simple shear flow (a) and in an elongational flow (b).

2.2.1. Characterization of Dispersive Mixing

A well-known parameter commonly used to evaluate the flow pattern in viscous fluid flows is the Manas-Zloczower index or mixing index [35]:

$$\lambda_{MZ} = \frac{|\boldsymbol{D}|}{|\boldsymbol{D}| + |\boldsymbol{W}|} , \tag{11}$$

where **D** and **W** are the rate-of-deformation tensor and the vorticity tensor, respectively denoting the symmetric and the asymmetric part of the velocity gradient tensor. The mixing index ranges from 0 to 1.0. In a Cartesian coordinate system, the following relationships are evident: (i) $\lambda_{MZ} = 0$ for pure rotational flow, (ii) $\lambda_{MZ} = 0.5$ for simple shear flow, and (iii) $\lambda_{MZ} = 1.0$ for elongational flow. When designing for dispersive mixing, the aim is to obtain a mixing index of 1.0. As this measure is not frame-invariant, it must be considered in combination with the magnitude of shear stresses [7].

3. Numerical Analysis

3.1. Geometry

Fig. 6 shows the set of block-head mixers analyzed in this design study. Three geometrical parameters were varied: (i) the number of flights at each block N_f, (ii) the number of blocks along the screw N_b, and (iii) the stagger angle between the blocks α_s. The scope of variation is summarized in Tab. 1. In all cases, the axial positions of the first and the last block, measured from the screw inlet to the center of the flight land, were kept constant at 47 mm and 158 mm, respectively. Additional characteristic dimensions are given in Tab. 2.

Table 1: Range of parameter values defined by minimum, maximum, and step size.

parameter	min	max	increment	comment
N_f	6	12	2	-
N_b	4	7	1	-
α_s	0°	+18°	+6°	positive displacement

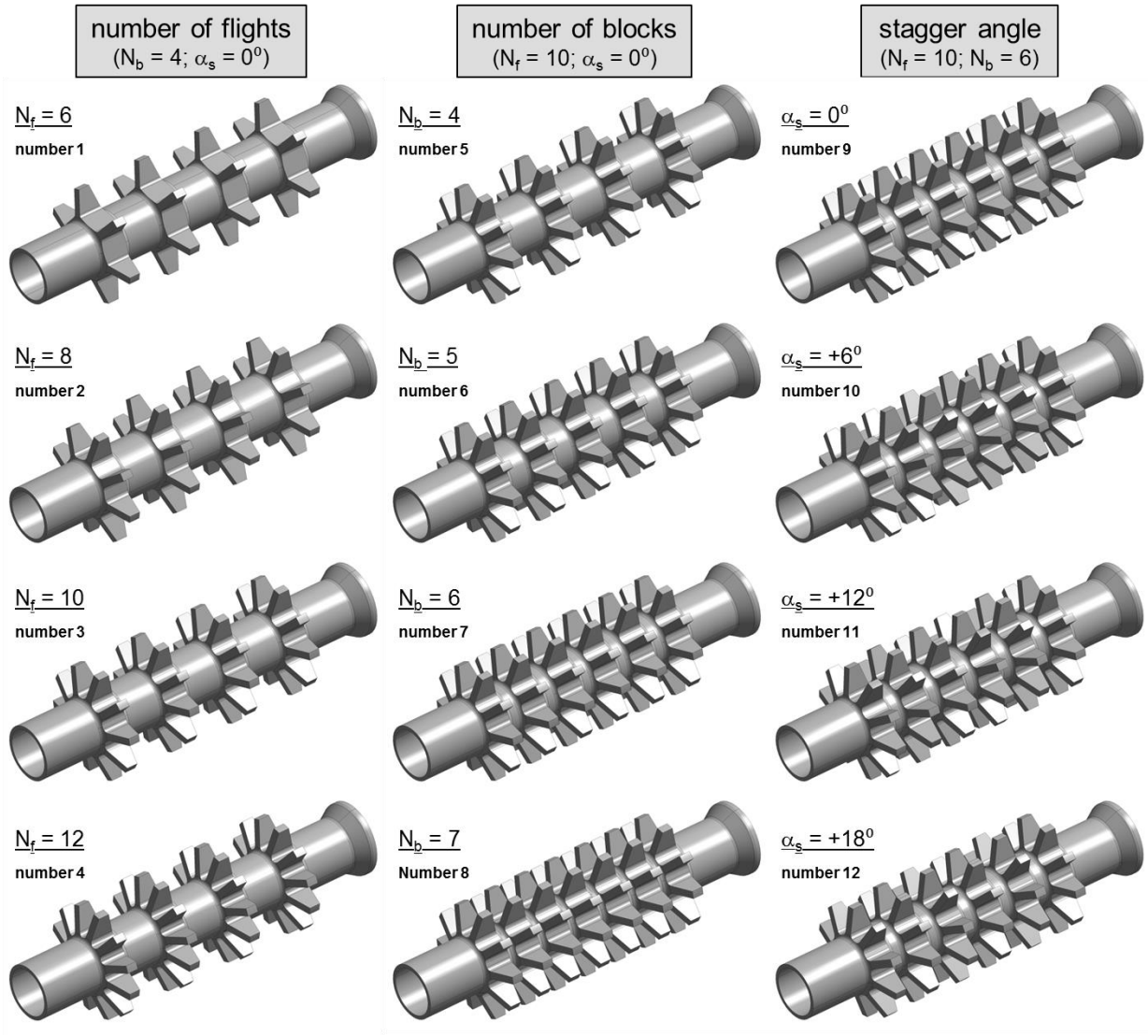

Figure 6: Set of block-head mixing screws. Three geometrical parameters were varied: (i) number of flights, (ii) number of blocks, and (iii) stagger angle.

For convenience, the geometry of the simple shaft was added to the set of block-head mixers. This geometry, which was designed with the same conical inlet and equal axial length, was used as reference configuration to demonstrate the effect of the screw flights on the flow and mixing performance.

Table 2: Geometrical data of the block-head mixers.

dimension	abbreviation	value	unit
axial screw length	L_{ax}	200.0	mm
barrel diameter	D_b	60.0	mm
screw tip diameter	D_o	59.6	mm
screw root diameter	D_i	29.0	mm
screw clearance	δ	0.2	mm
axial length of flight land	L_f	6.0	mm
width of flight land	w_f	4.0	mm

Block-head mixers are primarily distributive mixers that work by disrupting the flow in the screw channel, causing the molten streams to be split, reorientated and recombined multiple times. The main function of the flights is therefore to disturb and divide the flow passing through the mixing zone for thorough distributive mixing. Due to their deep flow channels, block-head mixers create relatively small levels of stresses and are thus not capable of dispersive mixing. Regions with high deformation rates are found in the clearances between the flight lands and the barrel surface. The mixing performance of block-head mixers strongly depends on the flow pattern in the screw channel, which is generally a combination of shear and elongational flow. The magnitude of these flow components is affected by the number and distribution of the screw flights. Yao [36] applied a kinematic approach to comparing pin-type mixing sections with different axial gaps and showed that the mixing performance reaches a level of saturation if the axial distance becomes too large.

3.2. Problem Definition

To analyze the flow and mixing behavior of the mixing screws under consideration, a computational design study was carried out. The following assumptions on the modeling set-up were made: (i) the flow is stationary and isothermal, (ii) the fluid is incompressible, and (iii) gravitational forces are negligible. The governing equations for the conservation of mass and momentum (given in [37]) are thus reduced to:

$$\nabla \cdot \left(\rho_m \right) = 0 , \tag{12}$$

$$\nabla \cdot \left(\rho_m \boldsymbol{v} \boldsymbol{v} \right) = -\nabla p + \nabla \cdot \boldsymbol{\tau} , \tag{13}$$

where ρ_m is the melt density, $\mathbf{v}$ the velocity vector, p the hydrostatic pressure, and $\boldsymbol{\tau}$ the stress tensor. Note that flows in polymer extrusion are generally dominated by internal friction rather than by inertial forces, that is, the Reynolds number is usually small (Re << 1). For this reason, viscous effects governed by the viscosity of the polymer melt and the deformation rates in the screw channel predominate. The following non-linear constitutive equation was used to describe the stress responses of the polymer melt being deformed:

$$\boldsymbol{\tau} = 2\eta\left(\dot{\gamma}\right)\boldsymbol{D} , \tag{14}$$

where the rate-of-deformation tensor **D** results from the symmetric part of the velocity gradient tensor:

$$\boldsymbol{D} = \frac{1}{2}\left(\nabla \boldsymbol{v} + \nabla \boldsymbol{v}^{\mathrm{T}}\right). \tag{15}$$

In order to take the shear-thinning nature of the fluid into account, the flow behavior of the polymer melt was represented by a Carreau-Yasuda model [38,39]:

$$\eta\left(\dot{\gamma}\right) = \frac{\eta_0 \cdot a_{\mathrm{t}}}{\left(1+\left(\lambda \dot{\gamma} a_{\mathrm{t}}\right)^{a}\right)^{\frac{1-n}{a}}}, \tag{16}$$

where η_0 is the zero-shear viscosity, λ the characteristic relaxation time, and n the power-law index. The parameter a = 1 defines the width of the transition between the Newtonian plateau and the shear-thinning region. The shear rate in three-dimensional flows is obtained from:

$$\left|\dot{\gamma}\right| = \left(2\left(\boldsymbol{D}:\boldsymbol{D}\right)\right)^{\frac{1}{2}}. \tag{17}$$

Two polymer melts with different rheological behaviors were compared: a high-density polyethylene (MFR = 0.25 g/min) and a polypropylene random copolymer (MFR = 8.0 g/min). In industry, the first material is applied in pipe extrusion processes, whereas the second material is typically found in the manufacturing of films. Tab. 3 shows the flow properties of both materials. The parameter values for the Carreau-Yasuda model were fitted from experimental viscosity data, as shown in Fig. 7, and shifted to a reference temperature of T_0 = 200°C. The temperature-shift factor was calculated from:

$$a_{\mathrm{t}} = \exp\left(-\alpha\left(T - T_0\right)\right), \tag{18}$$

where α is the temperature coefficient of the viscosity. In the following analysis, the more viscous polyethylene is referred to as material 1 and the less viscous polypropylene as material 2.

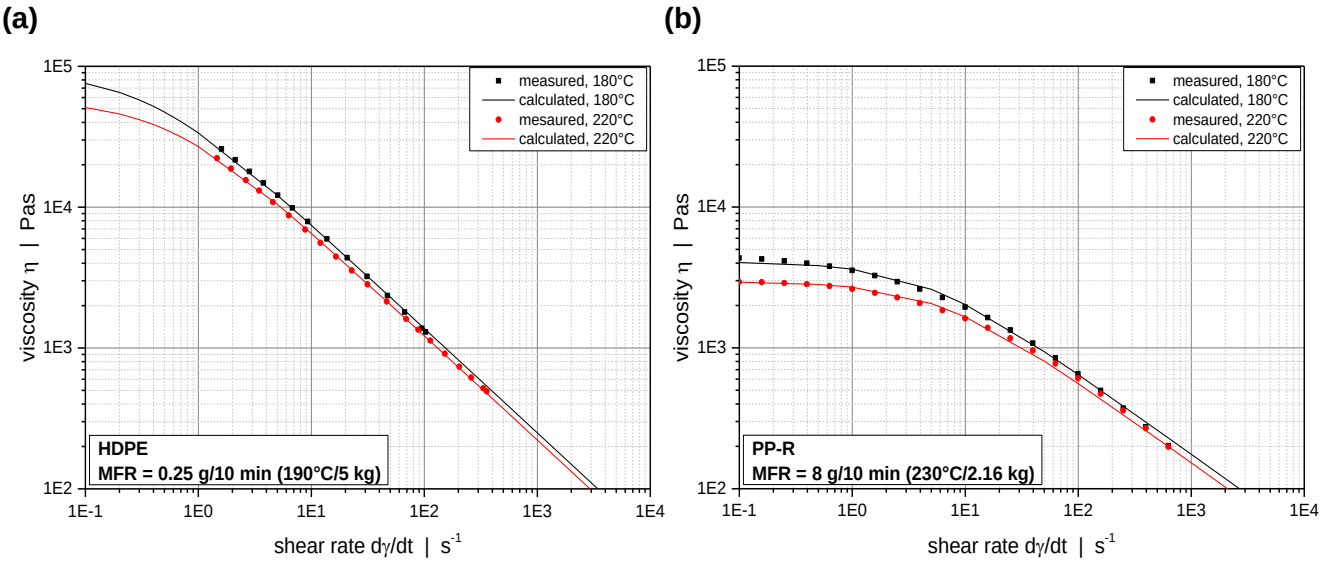

Figure 7: Viscosity data of the high-density polyethylene (a) and the polypropylene random copolymer (b) at temperatures of 180°C and 220°C. Comparison of measured and calculated values.

Table 3: Material data used in the simulations.

property	material 1	material 2	unit
η_0	72,452	2,957	Pas
λ	2.249	0.173	s
n	0.258	0.425	-
a	1	1	-
α	0.012	0.016	-
ρ_m	875	739	kg/m^3

3.3. FEM Approach

The governing flow equations were solved using the commercial software package ANSYS Polyflow 18.1, which is based on the finite-element method. To simplify mesh generation, the mesh superposition technique proposed by Avalosse and Rubin [15] was applied. Details of the modeling approach are given in [40]. The general procedure is the following: The meshes of the flow domain and the mixing screw are created separately and then superimposed, as illustrated in Fig. 8. At each time step, the algorithm updates the position of the rotating mixing element and detects whether a node of the flow domain is covered by the moving part. A penalty force term H($\mathbf{v}$-$\mathbf{v}_p$) added to the momentum equation is introduced to capture the velocity of the screw in the mathematical formulation:

$$H\left(\boldsymbol{v}-\boldsymbol{v}_{\mathrm{p}}\right)+\left(1-H\right)\left(-\nabla p+\nabla\cdot\boldsymbol{\tau}-\nabla\cdot\left(\rho_m\,\boldsymbol{v}\boldsymbol{v}\right)\right)=0\,, \tag{19}$$

where $\mathbf{v}_p$ is the velocity of the block-head mixer. The step function H provides the mathematical switch between fluid motion and rigid part motion, assuming values of either 0 or 1 outside or inside the moving part, respectively. Note that a stationary reference frame is considered. In the discretized flow configuration, both meshes overlap in the boundary area of the superimposed geometries. The location of this boundary is only known up to one mesh cell thickness. By default, a node of the flow domain is considered to be covered by the screw if more than half of the neighboring sub-elements are overlapped. To avoid non-physical pressure peaks in the sections where geometrical penetration occurs, the continuity equation is modified, allowing the fluid to be slightly compressible:

$$\nabla\cdot\boldsymbol{v}+\frac{\beta}{\eta\left(\dot{\gamma}\right)}\Delta p=0\,, \tag{20}$$

where β = 0.01 is the relative compression factor. Thus, the divergence-free condition of the velocity field is not fulfilled in all elements.

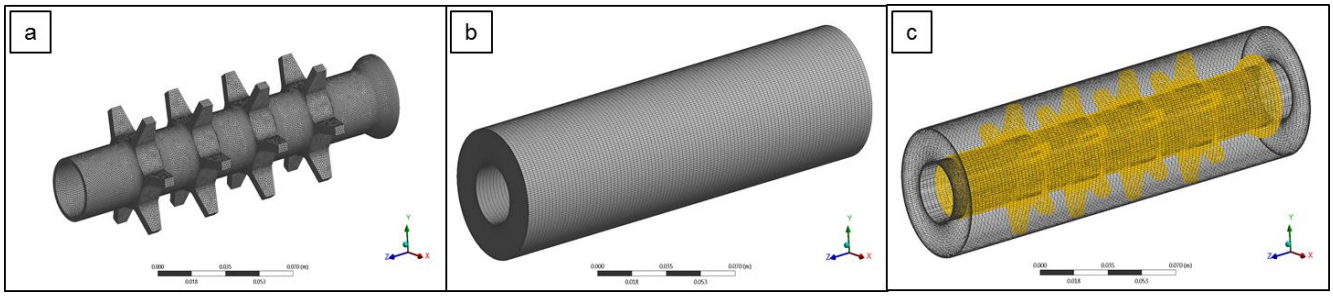

Figure 8: Mesh superposition technique. The meshes of the moving part (a) and the flow domain (b) are superimposed to obtain the final flow configuration (c).

In relation to boundary conditions, a constant mass flow rate of $\dot{m}$ = 500 kg/h was simulated at a screw speed of N = 200 rpm to model a high-rate extrusion process with a specific mass flow rate of 2.5 kg/h.min. Drawing on traditional extrusion theory [1], the no-slip condition was applied, assuming the polymer melt to adhere to the walls of the barrel and the rotating screw. To avoid incompatibilities in boundary conditions, the inlet and outlet sections of the flow domain were extended by 10 mm. A constant normal force with free tangential velocities was set at the flow entry, whereas normal and tangential forces were imposed at the flow exit. An isothermal flow being considered, the energy equation was omitted in the solving process, and thus the influence of thermal effects on viscosity was ignored. To estimate the temperature development in the screw channel, viscous dissipation, describing the amount of mechanical energy transformed into heat due to inner friction, was evaluated as follows:

$$\dot{q}_{\text{diss}} = \boldsymbol{\tau} : \nabla \boldsymbol{v} \,. \tag{21}$$

The nonlinearities in the governing flow equations introduced by the shear-rate dependency of the viscosity were solved using a Picard scheme. This viscosity-related iteration technique provides good convergence behavior if the power-law index in the Carreau-Yasuda model is low (n < 0.7 [40]). To calculate velocity and pressure field, enriched linear elements for the velocity (mini-element) were applied in combination with linear pressure elements. In the mini-element representation [41], nodes are added on the center of each face of each element (see Fig. 9). Due to the additional degree of freedom, this scheme strikes a reasonable balance between computational effort and accuracy. A result was considered converged when the relative error between two iteration steps was smaller than 0.001 and when all fields were taken into account.

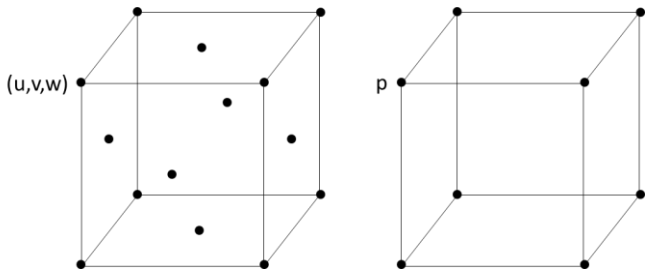

Figure 9: Interpolation models.

To assess distributive mixing in this design study, a particle tracking analysis was performed. For this purpose, 5,000 massless particles were generated randomly at the screw inlet, and their trajectories were calculated from the velocity field. Interaction between the material points was ignored. Statistical mixing parameters were then obtained by tracking the flow history of each particle. The simulations were carried out on a HP Z800 workstation at the Polymer Engineering Center at UW-Madison (Wisconsin, USA), using two Intel Xeon X5570 processors with 2.93 Ghz and 96 GB of installed memory (RAM).

3.4. Mesh Refinement Study

A mesh refinement analysis based on mixing screw 1 was carried out to find an accurate mesh for the simulations of the block-head mixers. Tab. 4 shows the mesh designs examined (16 grids in total). Tetrahedral elements were used to discretize the geometry of the mixing screw, whereas hexahedral elements were applied in the meshing of the flow domain. In the former case, the mesh distribution was controlled using a proximity and curvature size function. To reduce mesh size and thus save

computational costs, only a thin part of the outer contour of the mixing head was meshed. Note that the volume covered by the moving part does not influence the solution of the flow field. Four parameters were varied: (i) the global minimum size of the tetrahedral elements in the mesh of the mixing screw L_{min} (used in the proximity size function calculations), and (ii)-(iv) the number of hexahedral elements in the radial, tangential, and axial directions in the mesh of the flow domain N_{rad}, N_{tan}, and N_{ax}. In each case, one of these measures was modified, whereas all other quantities were kept constant.

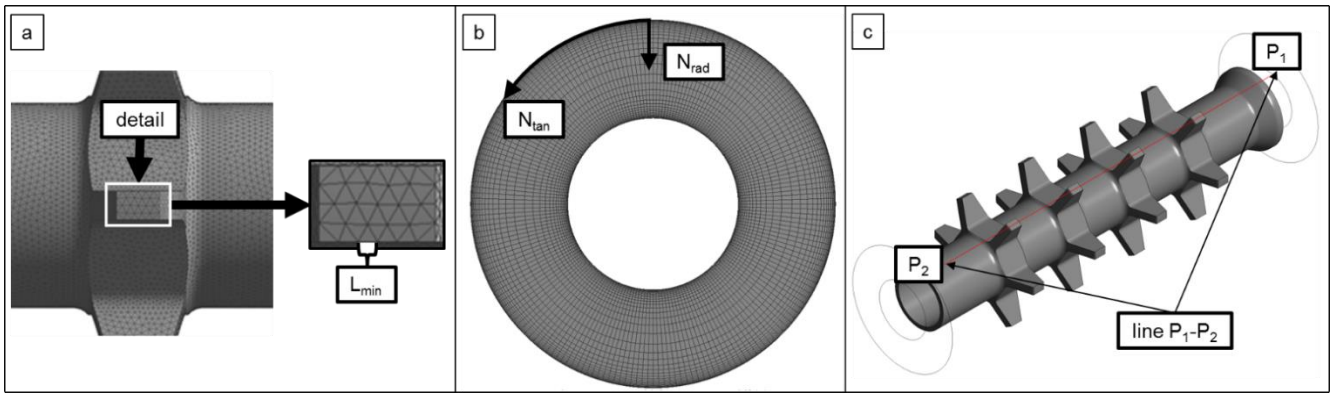

Figure 10: Side view of mixing screw with L_{min} = 1.00 mm (a), front view of flow domain with N_{rad} = 30 and N_{tan} = 250 (b), and position of line P_1-P_2 used for calculation of the pressure profiles (c).

The global minimum size of the tetrahedral elements was varied from 1 mm to 2 mm, yielding 3 to 6 elements in the axial direction of the flight land (see Fig. 10 (a)). Discretization of the flow domain was achieved as follows: A non-uniform mesh law was applied in the radial direction to provide a coarse cell distribution in the center with refinements in the vicinity of the inner and outer walls, resolving the large gradients in these areas (see Fig. 10 (b)). The number of elements in the radial direction was varied from 20 to 35, using three elements for the discretization of the clearance between the screw flight and the barrel in each case. In contrast, a uniform cell distribution was employed in the tangential and axial directions, where the number of elements was varied from 100 to 250 and from 75 to 150, respectively. Convergence tests were carried out by evaluating the pressure evolution along the line P_1-P_2 (see Fig. 10 (c)).

Table 4: Mesh designs. The gray fields show the parameter values selected for the design study.

	mixer	flow domain		
	L_{min}	N_{rad}	N_{tan}	N_{ax}
	mm	-	-	-
case 1	1.00	30	200	100
	1.25			
	1.50			
	2.00			
case 2	1.00	20	200	100
		25		
		30		
		35		

	mixer	flow domain		
	L_{min}	N_{rad}	N_{tan}	N_{ax}
	mm	-	-	-
case 3	1.00	30	100	100
			150	
			200	
			250	
case 4	1.00	30	200	75
				100
				125
				150

Fig. 11 illustrates the pressure profiles obtained from the mesh refinement study. The vertical dash-dotted lines represent the axial centers of the flight lands. As indicated by a negative pressure gradient, the pressure decreases along the block-head mixer. This pressure-reducing behavior is characteristic of grooved-feed extruders, in which pressure development takes place in the solids-conveying zone, causing the downstream functional zones to be overridden. The negative pressure gradient in these feed-controlled processes promotes transport of the material, yielding higher conveying rates compared to smooth-bore extruders. Note that the absolute pressure at the flow exit set by the boundary conditions does not affect the flow field, and the pressure profiles can be shifted vertically if this value changes, for example, in the presence of a die.

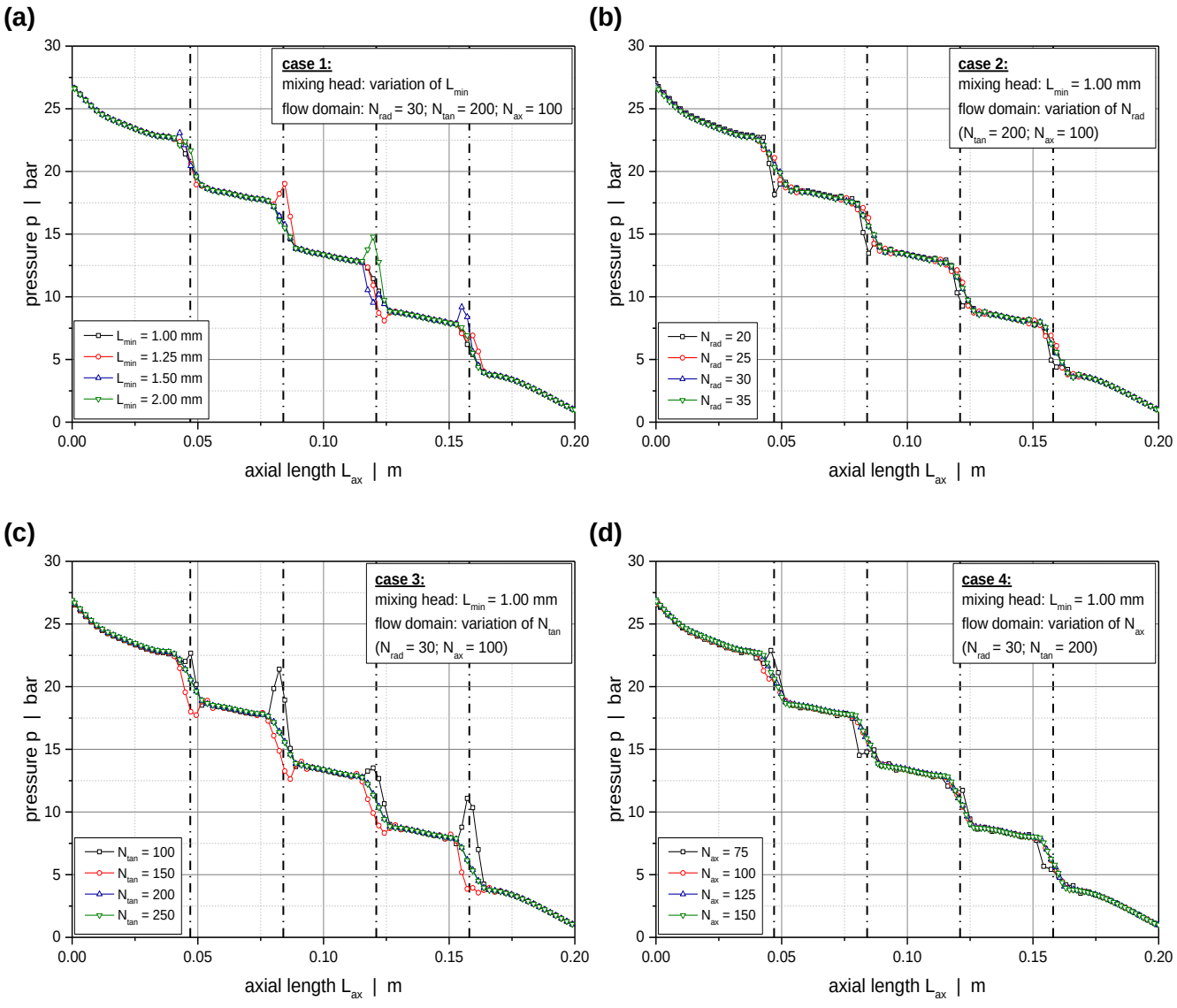

Figure 11: Pressure profiles along the line P_1-P_2 for material 1. Four parameters were varied: (a) the global minimum size of the tetrahedral elements L_{min}, and the number of hexahedral elements in the radial direction N_{rad} (b), in the tangential direction N_{tan} (c), and in the axial direction N_{rad} (d).

Clearly, the greatest pressure drops are found in the flight clearances due to the relatively small channel height. In these regions, the influence of the mesh design on the accuracy of the solutions is particularly pronounced. In contrast, the results in the remaining sections of the flow domain are nearly independent of mesh size. To obtain a fully converged pressure field, the following mesh parameters

were used in the design study: L_{min} = 1 mm, N_{rad} = 30, N_{tan} = 200, and N_{ax} = 125. With these settings, meshes consisting of approximately 1,300,000 to 1,600,000 bricks were created.

4. Results

4.1. Flow Field

To increase the general understanding of the flow in block-head mixers, three contour plots showing the flow pattern of mixing screw 1 are illustrated in Fig. 12. This device consists of four mixing blocks, each of which is equipped with six flights, and the stagger angle between the blocks is zero.

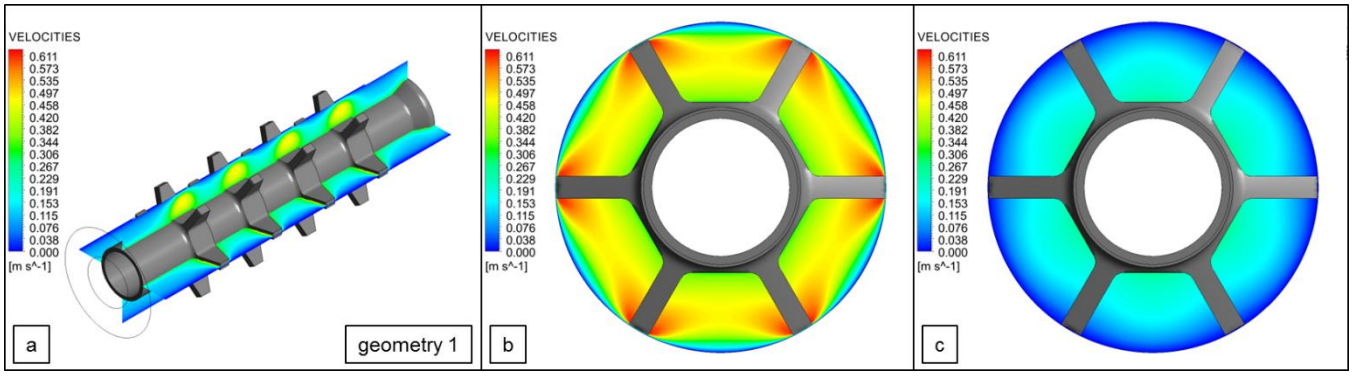

Figure 12: Contour plots of the flow field for material 1, showing the velocity distributions along the mixing head (a), in the axial cross section of a mixing block (b), and in the axial cross section between the mixing blocks (c).

The primary function of the screw flights is to disrupt the flow field to achieve thorough distributive mixing. Fig. 12 (a) demonstrates this effect by indicating a considerably non-uniform velocity distribution in the axial direction. Fluid elements passing through the block-head mixer exhibit a significant change in velocity due to the continuous change in free cross-sectional area. Local velocity peaks are found in the tangential center between two flights with velocities approximately three times higher than in the preceding annulus. A similar flow pattern is found in the cross section of a mixing block (see Fig. 12 (b)). Here, fluid elements are accelerated and decelerated in the tangential direction shortly before and after crossing the flight clearances, respectively. In contrast, the annular flow sections between the mixing blocks lack significant velocity gradients in the tangential direction (see Fig. 12 (c)).

4.2. Pressure Consumption

The pressure consumption of all block-head mixers is shown in Fig. 13 (a-c). The most critical parameter is the number of flights at each block. Installing a higher number of flights at the same axial position affects the pumping characteristics more distinctively than applying additional blocks along the screw or providing tangential displacement between the discs. This result is mainly due to the sensitivity of the pressure flow to the channel geometry. Ignoring the drag flow in the screw channel, two effects become evident. First, the pressure flow in annular ducts is more sensitive to the height of the flow channel than to its length; and second, the pressure gradient in the developing flow field is proportional to the viscosity of the fluid [42]. Consequently, to achieve the same throughput, the more viscous material requires a higher pressure gradient. The influence of the screw geometry on the pumping characteristics, however, is more pronounced in the case of the material with lower viscosity. This result is highlighted particularly in Fig. 13 (a), where doubling of the flight number increases pressure consumption by almost 60%. This result is due to the difference in rheological behavior between the two materials. An analysis of the viscosity curves in the region of shear rates slightly below 10 s^{-1} shows that the more viscous material is still highly shear-thinning, whereas the less

viscous material starts to drift into the Newtonian plateau (see Fig. 7). Note that these low shear rates make up a considerable proportion of the overall shear-rate distribution. Interestingly, the stagger angle between the blocks has almost no influence on the pressure consumption.

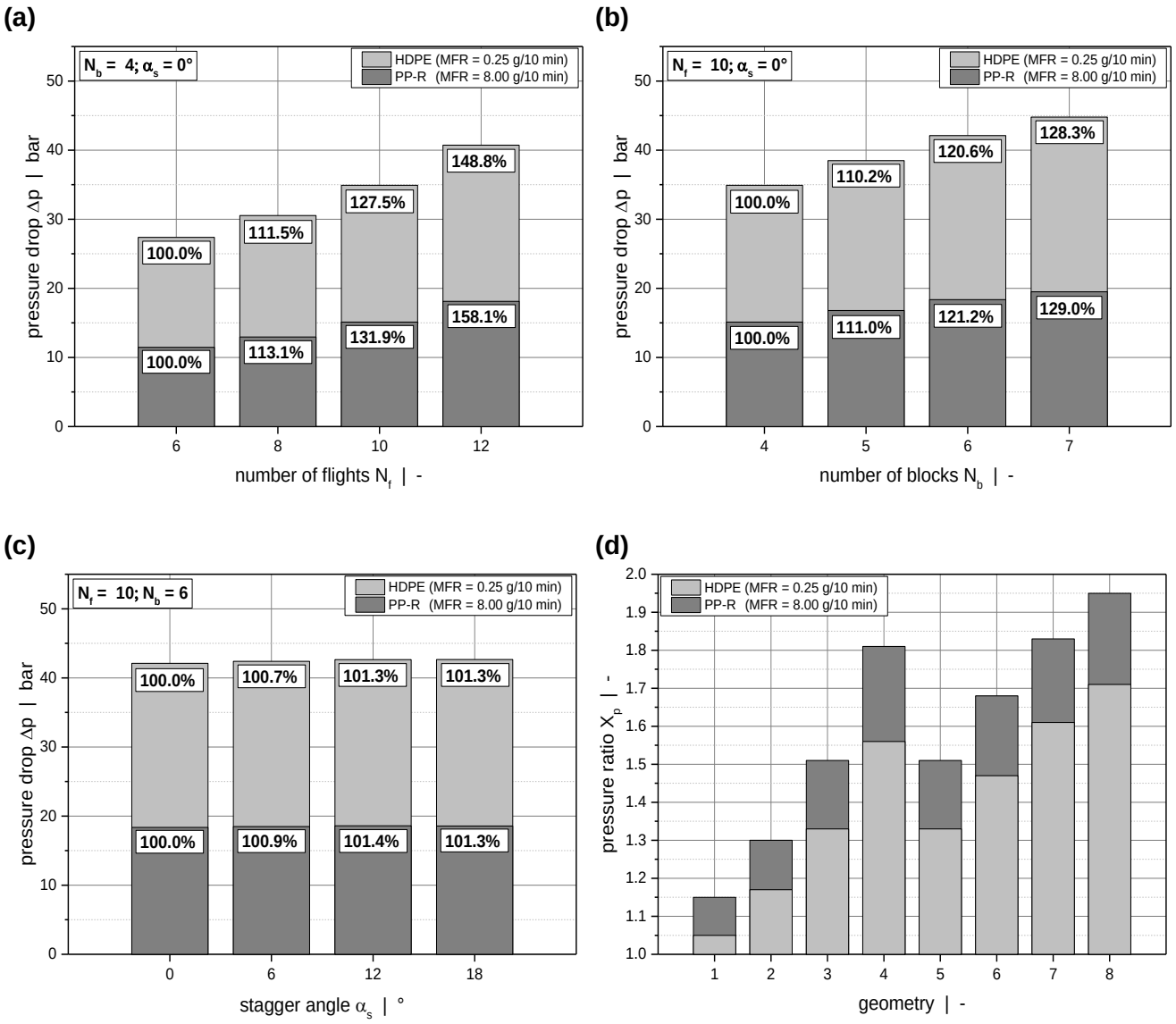

Figure 13: Pressure consumption of the block-head mixers 1-12: Variation of number of flights (a), number of blocks (b), and stagger angle (c). Pressure ratios evaluated for mixing screw 1-8 (d).

To estimate the influence of the screw flights on the pressure consumption, the following ratio is introduced, relating the pressure drop of each mixing screw to the results of the simple shaft (Δp_0 = 26.2 bar for material 1 and Δp_0 = 10.0 bar for material 2):

$$X_p = \frac{\Delta p}{\Delta p_0}. \tag{22}$$

The first two geometries exhibit nearly the same pressure drop as the shaft, as indicated in Fig. 13 (d), and therefore these designs can be considered as almost pressure-neutral.

4.3. Viscous Dissipation

Another important parameter in the analysis of extruder screws is viscous dissipation, which is mainly responsible for the temperature development in the screw channel. Due to inner friction between adjacent fluid layers, mechanical energy supplied from the rotating screw is converted into heat, causing a rise in melt temperature. The magnitude of viscous heating is proportional to the viscosity of the polymer melt and the deformation rates to which the polymer chains are exposed. The highest shear rates in the flow domains under consideration are found in the clearances between the flight lands and the barrel surface, with values in the range of 2,500 s^{-1}. Fig. 14 (a-c) compares the volume-average energy dissipation of all flow configurations.

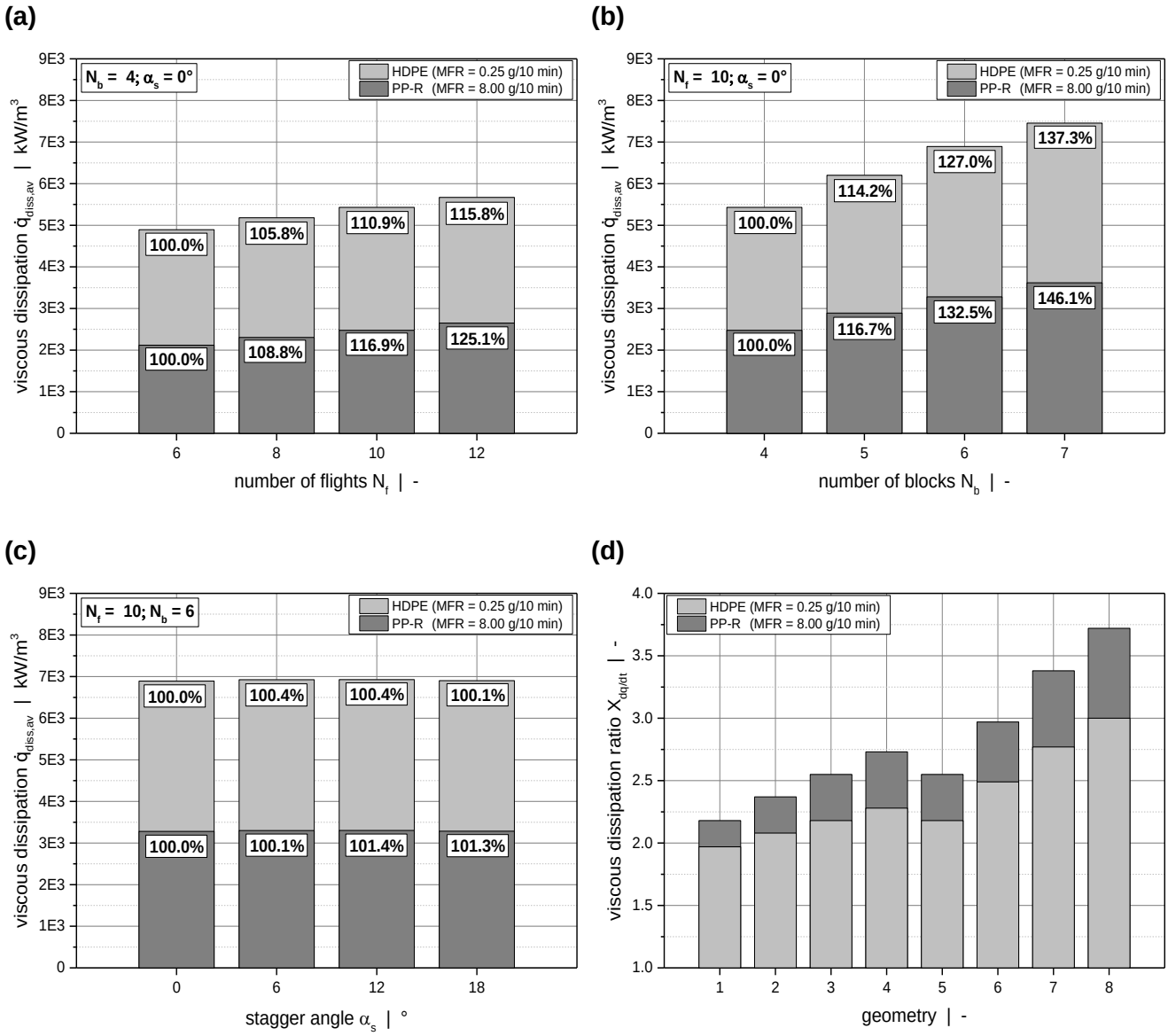

Figure 14: Volume-average energy dissipation of the flow domains 1-12: Variation of number of flights (a), number of blocks (b), and stagger angle (c). Viscous dissipation ratio calculated for mixing screws 1-8 (d).

Viscous dissipation is governed primarily by the number of mixing blocks along the screw. Clearly, a higher number of blocks simultaneously increases the number of flight clearances, thus providing a higher level of viscous heating. The effect of frictional heat generation is particularly pronounced if the viscosity of the polymer melt is high, yielding values that are approximately twice as high for the more

viscous material. This result is in good agreement with the rheological data in Fig. 7, where the viscosity curves differ by a factor of about two in the relevant region of volume-average shear rates ($40 < \dot{\gamma} < 50\ s^{-1}$). Comparing the dissipated energies of the two materials shows that the less viscous polymer melt exhibits a greater sensitivity to number and distribution of the screw flights. This result is due to the additional pressure gradient needed and the different rheological behaviors of the two materials. The influence of the stagger angle on viscous heating is, again, relatively small. As in the previous case, a characteristic ratio is defined that relates the energy dissipation of each mixing head to the results of the simple shaft ($\dot{q}_{diss,av,0} = 2487\ kW/m^3$ for material 1 and $\dot{q}_{diss,av,0} = 971\ kW/m^3$ for material 2):

$$X_{\dot{q}} = \frac{\dot{q}_{\mathrm{diss,av}}}{\dot{q}_{\mathrm{diss,av,0}}}\,. \tag{23}$$

The results, which allow the influence of the screw flights on viscous heating to be estimated, are shown in Fig. 14 (d).

4.4. Dispersive Mixing

Due to their deep flow channels, block-head mixers generally create low levels of stresses. Regions of high stresses are generated in the clearances between the flight lands and the barrel surface, with maximum values in the range of 310 kPa and 240 kPa for the more and the less viscous materials, respectively. The flow in these narrow channel gaps is governed predominantly by shear, as indicated by a mixing index of 0.5. To achieve efficient dispersive mixing, however, elongational flow is preferable, since the hydrodynamic forces are higher than in shear flows [32]. To demonstrate the dominant flow pattern in the block-head mixers under consideration, the volume-average mixing index of the flow domains 1-8 is shown in Fig. 15. Note that the effect of the stagger angle on the mixing index is relatively small, and for this reason geometries 9-12 are excluded from the presentation of the results below.

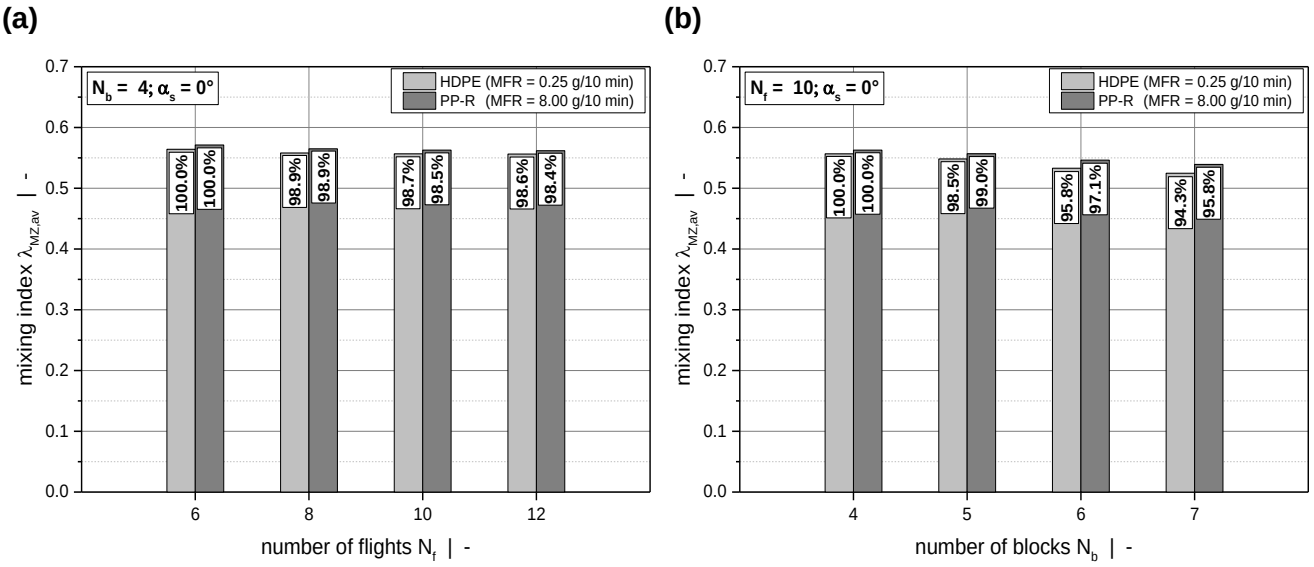

Figure 15: Volume-average mixing index of the flow configurations 1-8: Variation of number of flights (a) and number of blocks (b).

The average mixing index decreases with increasing numbers of flights and mixing blocks almost identically for both materials. Especially in the latter case, the reduction is significant, considering that the average values were calculated for the entire flow domain. An explanation for this decrease can be found in Fig. 16 (a-c), where contour plots illustrate the axial distribution of the mixing index along the simple shaft, geometry 5, and geometry 8.

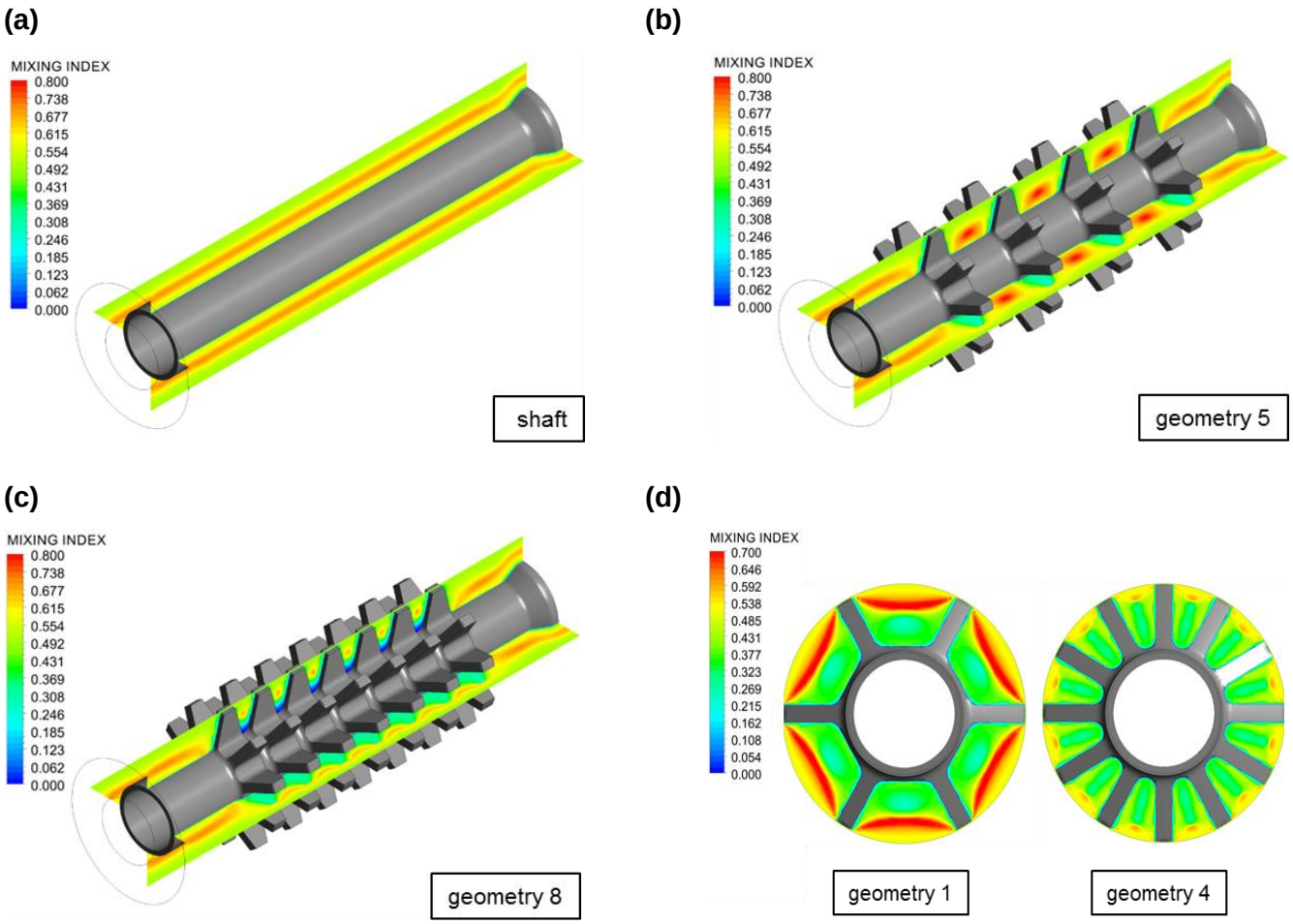

Figure 16: Contour plots of the axial distribution of the mixing index for material 1, showing the simple shaft (a), geometry 5(b), and geometry 8(c).

The highest mixing indices are found in the annuli between the mixing blocks, with values around 0.8, which indicates a significant proportion of elongational flow. Fluid elements in these regions exhibit a considerable velocity gradient in the axial direction, and are thus being constantly accelerated and decelerated (see Fig 12). This continuous change in velocity magnitude causes the fluid elements to be constantly stretched and folded, imposing extensional work on the polymer melt. Note that the axial distance between the mixing blocks must be sufficiently large to allow flow to reestablish. Placing the mixing blocks too closely together diminishes both the elongational flow components and the level of dispersive mixing. The mixing performance is also limited if the axial gap between the discs is too large, as the velocity gradients along the screw become less pronounced. A similar result is evident in the cross section of a mixing block (see Fig. 16 (d)). Increasing the number of flights at each block mitigates the extensional work imposed on the fluid between the screw flights. The fluid elements near the screw core show a significant proportion of rotational flow components, as indicated by a mixing index around 0.4. These regions do not contribute to the dispersive mixing

performance. Fig. 17 presents the volume-average shear stress for the geometries 1-8. In contrast to the mixing index, the average shear stress increases with increasing numbers of flights and blocks. This result is due to the presence of additional flight clearances, which compensate for the loss in extensional flow by generating high shear stresses. Note that, despite maintaining the average shear-stress level in the flow domain, this effect has a negative impact on pressure consumption and energy dissipation.

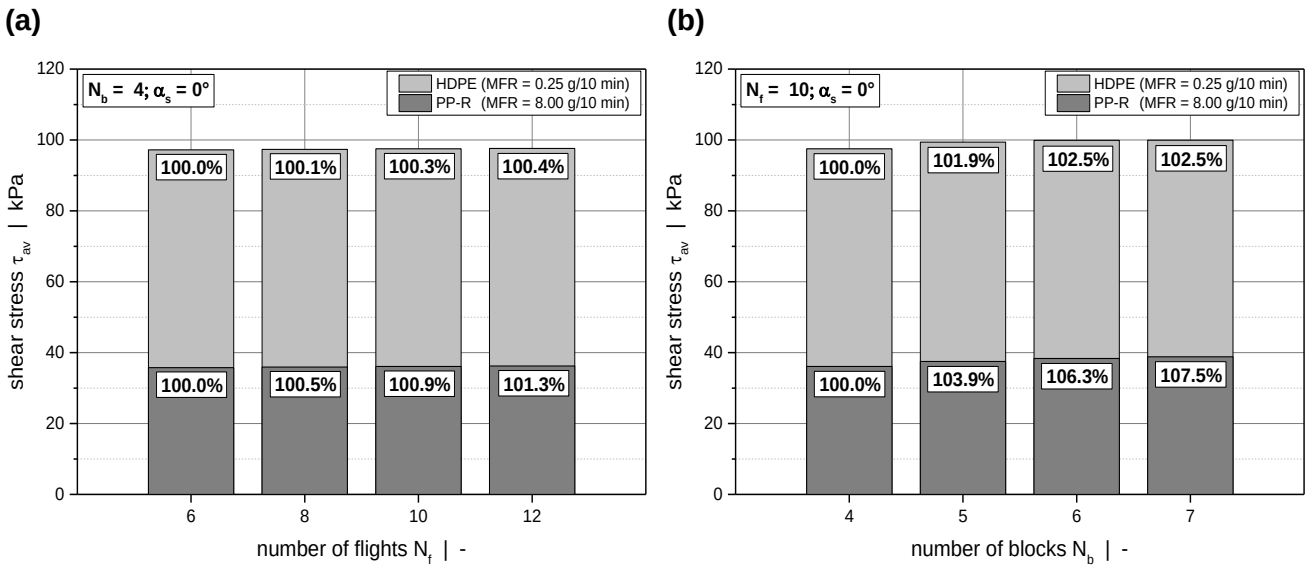

Figure 17: Volume-average shear stress of the flow domains 1-8: Variation of number of flights (a) and number of blocks (b).

The stress-compensating effect described above is demonstrated in detail in Fig. 18, which shows the volumetric distributions of the mixing indices and shear stresses for geometries 5 and 8. Increasing the number of mixing blocks decreases the proportion of mixing indices with values higher than 0.5, which indicates a loss in elongational flow. In contrast, the frequency of shear stresses with values higher than 50 kPa is increased due to the presence of additional high-shear zones in the newly created flight clearances.

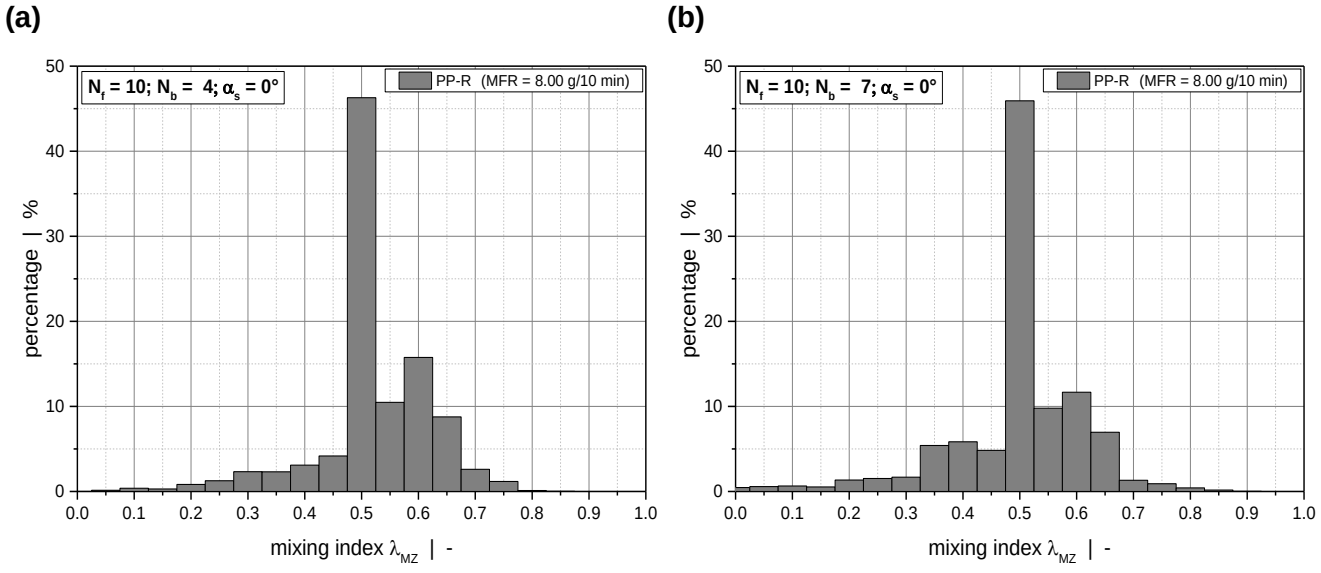

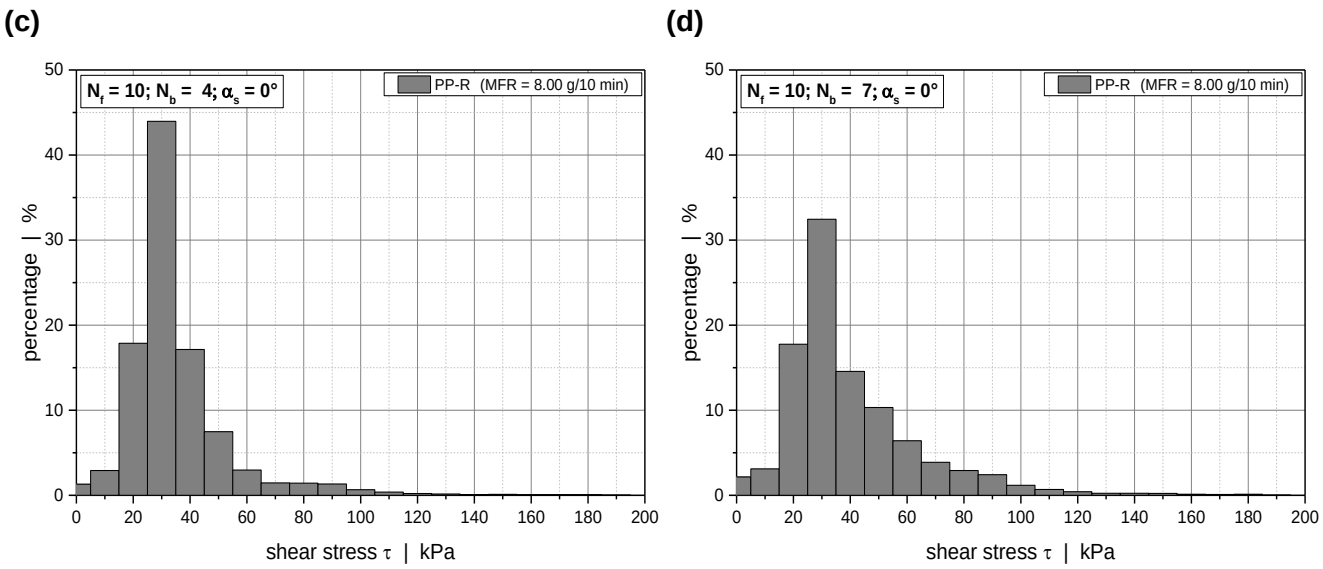

Figure 18: Volumetric distributions of the mixing indices and shear stresses for geometries 5 and 8 and material 1.

4.5. Distributive Mixing

To visually analyze distributive mixing in block-head mixers, the axial evolution of a concentration field defined at the beginning of the screw was evaluated for all mixing heads. To this end, all material points located in one half of the screw inlet were specified with a unit concentration (red particles), whereas the points in the remaining inlet plane received a null concentration (blue particles). To visualize the increase in interfacial area between the two colors, the concentration field was calculated along the trajectories, as shown in Fig. 19.

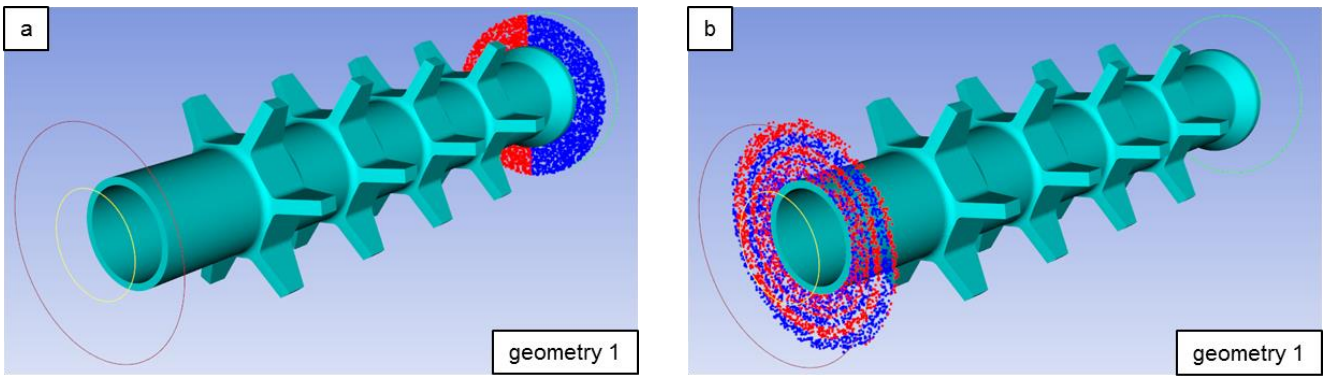

Figure 19: Concentration field at the screw entry (a) and the screw exit (b) for geometry 1 and material 1.

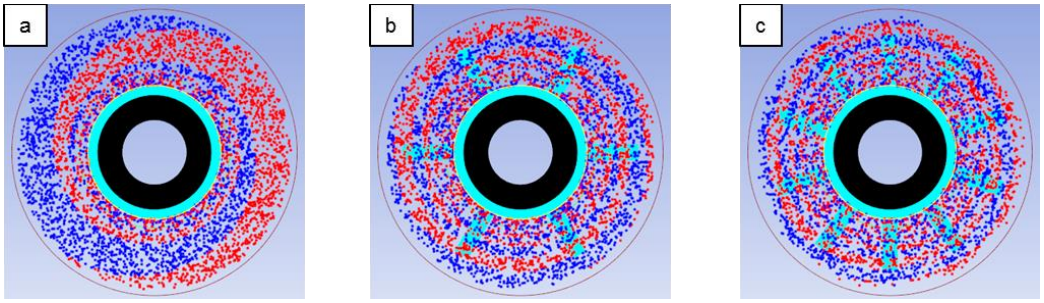

Figure 20: Concentration field at the screw exit for the simple shaft (a), geometry 1 (b), and geometry 8 (c).

The concentration fields at the end of the simple shaft, geometry 1, and geometry 8 are compared in Fig. 20. Distributive mixing improves as the material points move in the flow field. New striations are formed, and the average striation thickness of the mixture decreases while the interfacial area created by the mixing process increases [43]; this results in a finer concentration distribution at the outlet of the block-head mixers. The increase in interfacial area is less pronounced in the case of the simple shaft, where the velocity field lacks significant velocity gradients. A higher level of distributive mixing is achieved if the velocity field is constantly disrupted. In the case of block-head mixers, the presence of screw flights promotes reorientation of the surface elements, increasing the efficiency of distributive mixing. A qualitative difference between the mixing screws 1 and 8 is not evident from the visual representation in Fig. 20.

To quantify the evolution of the concentration field along the mixing screws, the scale of segregation was plotted over the axial length in Fig. 21 for the geometries 1-8 and material 1. The scale of segregation is a measure of the cross-sectional mixing capability. The parameter decreases significantly at the beginning of the mixing heads and tends to a plateau value of approximately 1 mm after 0.01 m (= 1.66 L_{ax}/D_b). The initial reduction is almost equal for all mixing screws. Minor differences are detected in the region between 0.06 m (= 1 L_{ax}/D_b) and 0.08 m (= 1.33 L_{ax}/D_b), where the densely packed geometries show improved distributive mixing. The final concentration distribution, however, is nearly equal for all screw designs. Consequently, cross-sectional mixing is not improved if the numbers of flights and blocks are increased. However, given the significant difference from the behavior of the simple shaft, the results suggest that geometry 1 is the most efficient mixing head, as it achieves the same final concentration field with the lowest number of screw flights. Further, the results indicate that cross-sectional mixing remains almost the same if the axial length of the block-head mixers is reduced by half. Similar results were obtained for material 2. The stagger angle was again found to be insignificant in this analysis. Note that the evolution of the segregation scale along the screw strongly depends on the initial concentration distribution. In single-screw extrusion, this distribution is usually unknown.

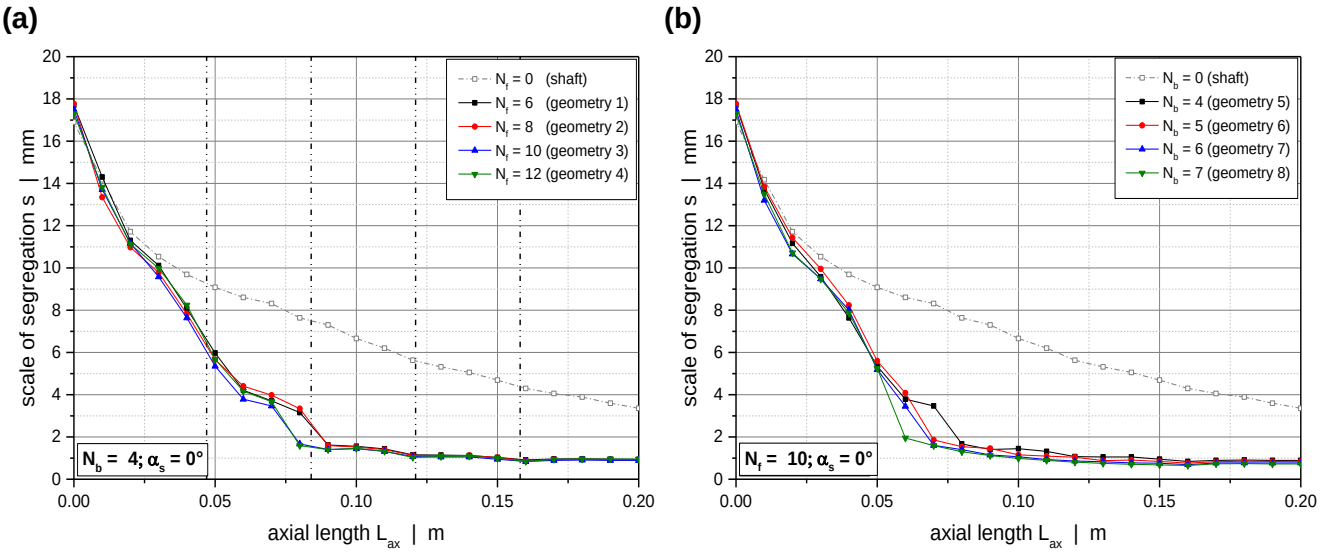

Figure 21: Axial evolution of the scale of segregation for material 1: Variation of number of flights (a) and number of blocks (b).

Distributive mixing in the axial direction was characterized by means of residence time distribution functions, as shown in Fig. 22. Given the high specific flow rate of the simulated process, the

residence time of the particles in the flow domains is relatively short, ranging from approximately 1.5 s to 15.0 s. These values represent the minimum and maximum residence times of the material points. The block-head mixer exhibits limited axial-mixing capability, as indicated by the narrow peaks in the residence time distributions. The performance can be slightly improved if the number of flights at each block is increased, which causes the flow to be divided more often. The effects of the mixing blocks and the stagger angle on axial mixing are not clearly evident. Notice that the self-cleaning time of the geometries defined as the difference between the maximum and the minimum residence times is comparatively high but similar in all cases investigated.

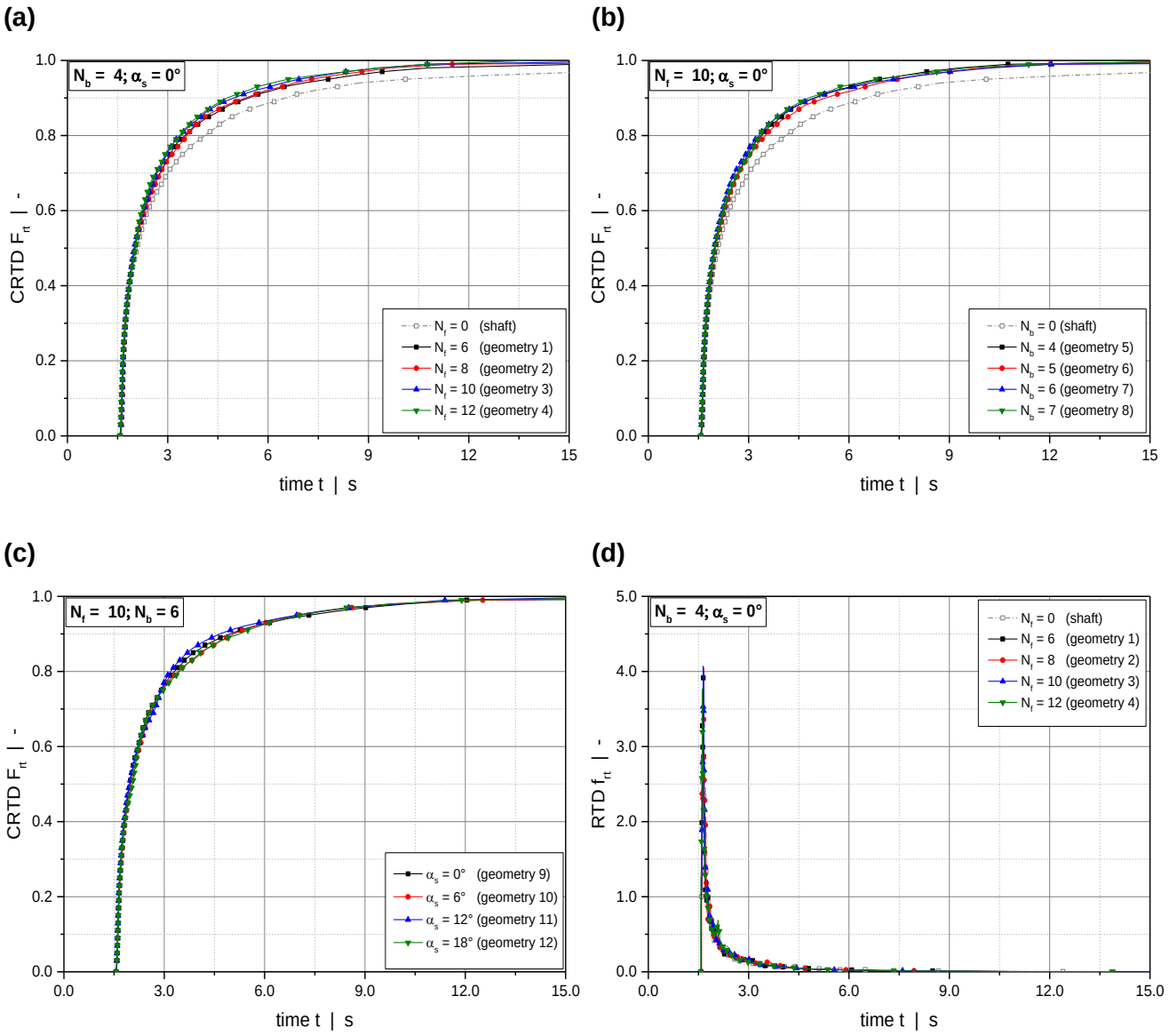

Figure 22: Cumulative residence time distribution functions for material 2: Variation of number of flights (a), number of blocks (b), and stagger angle (c). Residence time distribution functions for geometries 1-4 and material 2 (d).

4.6. Kinematic Analysis

To investigate mixing in block-head mixers from a kinematic viewpoint, the local area stretch and the stretching efficiency were calculated from the set of particles tracked in this analysis. The influence of the number and distribution of the screw flights on the mean values of these parameters is shown in Fig. 23. By taking the flow history of the material points into account, the local area stretch exhibits a sharp increase at the beginning of the mixing section, whereas the gradients of the curves decrease with increasing screw length and reach zero at the end of the screw. Physically, this means that stretching becomes less efficient as the particles move forward. Stretching improves as the number of flights at each block is increased (see Fig. 23 (a)). Note that a logarithmic scale was used to express the results. Decreasing the free cross-sectional area promotes the elongational flow in the annuli between the mixing blocks, causing reorientation of the fluid elements and thus an increase in stretching efficiency. In contrast, the stretching efficiency decreases as the material points pass through the mixing blocks. Here, the flow pattern shows a significant proportion of rotational flow components, which do not promote stretching of the fluid elements (see Fig. 23 (b)).

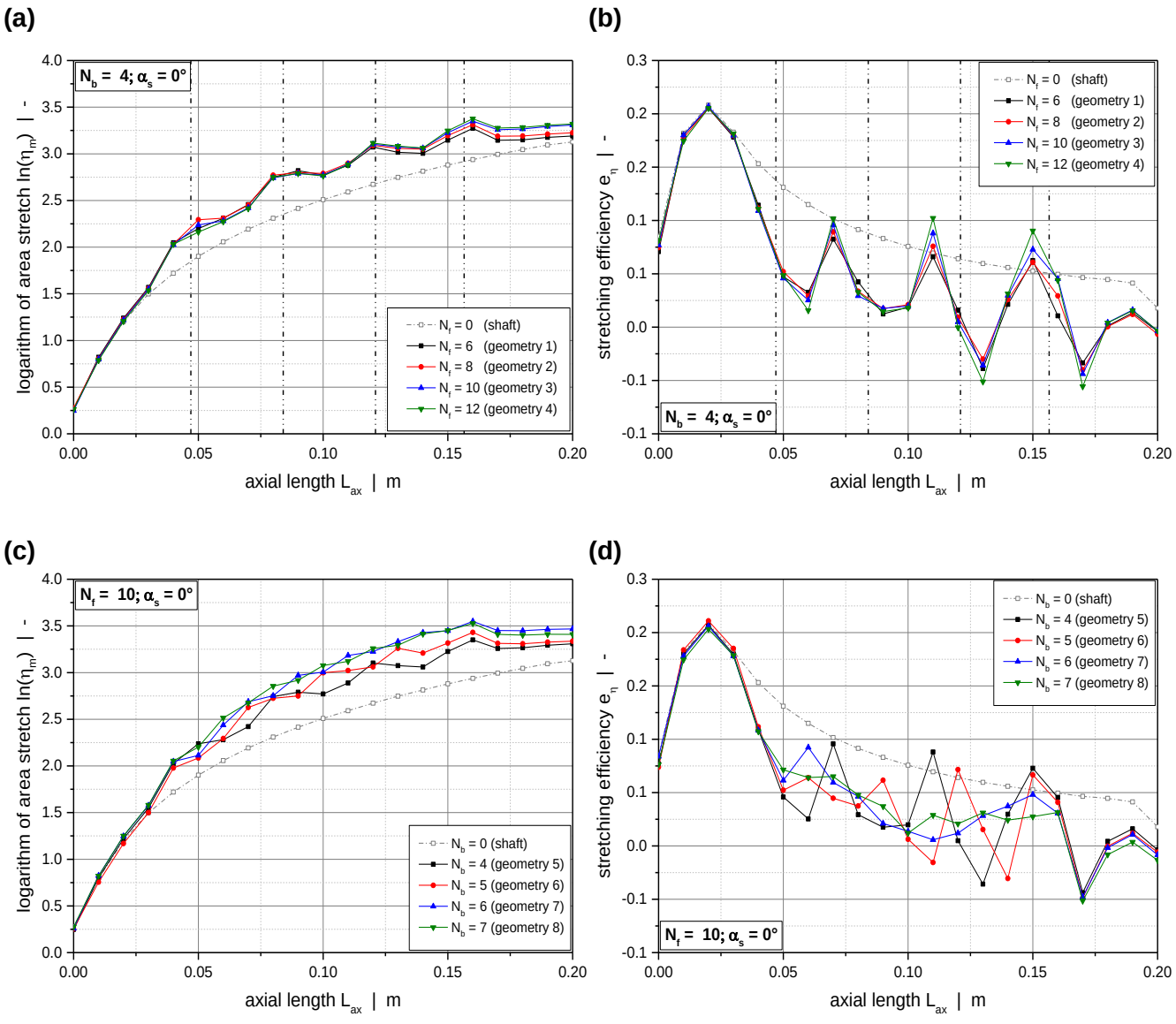

Figure 23: Axial evolution of the mean local area stretch and the mean stretching efficiency for material 1: Variation of number of flights (a) and number of blocks (b).

The stretching behavior is also affected by the number of mixing blocks along the screw. Stretching improves as more discs are installed, which increases the frequency of reorientation processes along the mixing head (see Fig. 23 (c)). This improvement, however, is limited by the axial distance between the discs. As in the analysis of dispersive mixing, a lower level of stretching is achieved if the mixing blocks are too close together. In this case, the axial fluctuations in stretching efficiency vanish, mitigating the reorientation processes between the mixing blocks (see Fig. 23 (d)).

6. Conclusion

This report has investigated the flow and mixing behaviors of block-head mixers by means of a computational design study. Using three-dimensional, non-Newtonian flow simulations, the influence of three geometrical parameters was investigated: (i) the number of flights at a mixing block, (ii) the number of blocks along the screw, and (iii) the stagger angle between the blocks.

Comparing two rheologically different materials, the analysis showed that the pressure consumption of block-head mixers depends mainly on the number of flights at the same axial position, whereas viscous dissipation is governed principally by the number of mixing blocks along the screw. Dispersive mixing was assessed by evaluating the mixing index and the shear stresses. It was observed that a critical parameter is the amount of extensional work imposed on the fluid elements, which can be controlled by the positioning of the screw flights. Of particular importance is the axial and tangential distance between the screw flights. Installing the flights too closely together significantly reduces the proportion of elongational flow, thus decreasing stretching and folding of the fluid elements. The mixing performance is also limited if the axial and tangential gaps between the screw flights are too large, as the velocity gradients providing constant acceleration and deceleration of the polymer melt become less pronounced. The loss in elongational flow reduces the average-stress level in the flow domain and can be compensated for by increasing the number of flights and thus the number of flight clearances. The flow through these narrow channel gaps is, however, governed by shear, and has thus a negative impact on energy dissipation and pressure consumption.

Distributive mixing was analyzed visually and by comparing the scales of segregation, residence time distribution functions, and kinematic stretching parameters. The cross-sectional and axial mixing capability was found to be almost equal for all block-head mixers under consideration. Minor improvements can be achieved if the number of flights at each block is increased, as this causes the flow to be split more often. Installing a higher number of mixing blocks along the screw slightly increases cross-sectional mixing, whereas no clear effects on axial mixing are evident. In contrast, the kinematic analysis shows that – taking the logarithmic representation of the results into account – stretching of the fluid elements is noticeably affected by the number and distribution of the screw flights. A significant parameter is again the amount of extensional work imposed on the fluid elements, which causes reorientation processes and therefore increases stretching efficiency.

7. Nomenclature

a	width of transition
a_t	temperature-shift factor
A	area
A_0	initial area
c_i', c_i''	concentration of the points of the i^{th} pair
c_{mean}	mean concentration
C	constant
$\mathbf{D}$	rate-of-deformation tensor
D_b	barrel diameter
D_i	screw root diameter
D_o	screw tip diameter
e_η	area stretching efficiency
f_{rt}	external residence time distribution function
F	force
F_{rt}	cumulative residence time distribution function
F_s	cumulative strain distribution function
f_s	strain distribution function
H	step function
L_{ax}	axial screw length
L_{min}	global minimum element cell size
L_f	axial length of flight land
M	number of pairs of points
n	power-law index
N	number of shearing sections
N_{ax}	number of elements in axial direction
N_b	number of blocks
N_f	number of flights
N_{rad}	number of elements in radial direction
N_{tan}	number of elements in tangential direction
p	pressure
$\dot{q}_{diss}$	viscous dissipation per unit volume
r	radius
R	coefficient of correlation
s	segregation scale
t	time
t_0	minimum residence time
T	temperature
T_0	reference temperature
$\mathbf{v}$	velocity vector
$\mathbf{v}_p$	velocity vector of moving part
w_f	width of flight land
$\mathbf{W}$	vorticity tensor
X_p	pressure ratio
$X_{\dot{q}}$	energy dissipation ratio
α_s	stagger angle

α_x, α_y, α_z	angles of orientation
β	compressibility factor
δ	screw clearance
γ	strain
γ_0	minimum strain
$\dot{\gamma}$	shear rate
η	viscosity
η_m	area stretch
η_0	zero-shear viscosity
λ	characteristic relaxation time
λ_{MZ}	mixing index
ρ_m	melt density
σ_s	sample variance
$\boldsymbol{\tau}$	stress tensor
τ_e	elongational stress
τ_s	shear stress

References

1. Tadmor, Z., Klein, I.: Engineering Principles of Plasticating Extrusion, Van Nostrand Reinhold, New York (1970)
2. Tadmor, Z., Gogos, Z.G.: Principles of Polymer Processing, 2nd Ed., Wiley & Sons, Inc., New Jersey (2002)
3. Campbell, G.A., Spalding, M.A.: Analyzing and Troubleshooting Single-Screw Extruders, Hanser Publishers, Munich (2013)
4. Rauwendaal, C.: Polymer Extrusion, 5th Ed., Hanser Publishers, Munich (2014)
5. Gale, M.: Mixing Single-Screw Extrusion, iSmithers, Shawbury (2009)
6. Manas-Zloczower, I.: Mixing and Compounding of Polymers – Theory and Practice, 2nd Ed., Hanser Publishers, Munich (2013)
7. Yang, H. H, Manas-Zloczower, I.: "Flow Field Analysis of the Kneading Disc Region in a Co-Rotating Twin Screw Extruder", Polym. Eng. Sci., 32, 1411-1417 (1992), DOI: 10.1002/pen.760321903
8. Cheng, H., Manas-Zloczower, I.: "Study of Mixing Efficiency in Kneading Discs of Co-Rotating Twin-Screw Extruders", Polym. Eng. Sci., **37**, 1082-1990 (1997), DOI: 10.1002/pen.11753
9. Yoshinaga, M., Katsuki, S., Miyazaki, M., Liu, L., Kihara, S. I. and Funatsu, K.: "Mixing Mechanism of Three-Tip Kneading Block in Twin Screw Extruders", Polym. Eng. Sci., 40, 168-178 (2000), DOI: 10.1002/pen.11150
10. Ishikawa, T., Kihara, S. I. and Funatsu, K.: "3-D Numerical Simulations of Nonisothermal Flow in Co-Rotating Twin Screw Extruders", Polym. Eng. Sci., **40**, 357-364 (2000), DOI: 10.1002/pen.11169
11. Ishikawa, T., Kihara, S. I. and Funatsu, K.: "3-D Non-Isothermal Flow Field Analyses and Mixing Performance Evaluation of Kneading Blocks in a Co-Rotating Twin Screw Extruder, Polym. Eng. Sci., **41**, 840-848 (2001), DOI: 10.1002/pen.10781
12. Bravo, V. L., Hrymark, A. N. and Wright: "Study of Particle Trajectories, Residence Times and Flow Behavior in Kneading Discs of Intermeshing Co-Rotating Twin-Screw Extruders", Poly. Eng. Sci., 44, 779-793 (2004), DOI: 10.1002/pen.20070
13. Ishikawa, T., Nagano, F., Kajiwara, T. and Funatsu, K.: "Tip-clearance Effect on Mixing Performance of Twin Screw Extruders", Int. Polym. Process., **21**, 354-360 (2006), DOI: 10.3139/217.0088
14. Rios, A. C., Gramann, P. J. and Osswald, T. A.: "Comparative Study of Mixing in Corotating Twin Screw Extruders Using Computer Simulation", Adv. Poly. Tech., **17**, 107-113 (1998), DOI: 10.1002/(SICI)1098-2329(199822)17:2<107::AID-ADV2>3.0.CO;2-X
15. Avalosse, T., Rubin, Y.: "Analysis of Mixing in Corotating Twin Screw Extruders through Numerical Simulation", Int. Polym. Process., **15**, 117-123 (2000), DOI: 10.3139/217.1586
16. Avalosse, T., Rubin, Y. and Fondin: "Non-Isothermal Modeling of Co-Rotating and Contra-Rotating Twin Screw Extruders", Journal of Reinforced Plastics and Composites, **21**, 419-429 (2002), DOI: 10.1177/0731684402021005442
17. Alsteens, B., Legat, V. and Avalosse, T.: "Parametric Study of the Mixing Efficiency in a Kneading Block Section of a Twin-screw Extruder", Int. Polym. Process., **19**, 207-217 (2004), DOI: 10.3139/217.1836
18. Bertrand, F., Tanguy, P. A. and Thibault, F.: "A Three-Dimensional Fictitious Domain Method For Incompressible Fluid Flow Problems", Int. J. Num. Meth. Fluids, **25**, 719-736, (1997), DOI: 10.1002/(SICI)1097-0363(19970930)25:6<719::AID-FLD585>3.0.CO;2-K

19. Wang, Y., Tsay, C. C.: “Non-Newtonian Flow Modeling in the Mixing Section of a Single-Screw Extruder With Flow Analysis Network Method”, Polym. Eng. Sci., **36**, 643-650 (1996), DOI: 10.1002/pen.10452
20. Kubik, P., Vlcek, V., Tzoganakis, C. and Miller, L.: “Method of Analyzing and Quantifying the Performance of Mixing Sections”, 52, 1232-1240 (2012), DOI: 10.1002/pen.22191
21. Sun, X., Spalding, M. A., Womer, T. W. and Uzelac, N.: “Design Optimization of Maddock Mixers for Single-Screw Extrusion Using Numerical Simulation”, SPE ANTEC Tech. Papers, 1017-1023 (2017)
22. Rios, A. C., Gramann, M. P., Osswald, T. A., Noriega M. P. and Estrada, O. A.: “Experimental and Numerical Study of Rhomboidal Mixing Sections”, Int. Polym. Process., **15**, 12-19 (2000), DOI: 10.3139/217.1578
23. Rauwendaal, C., Osswald, T., Gramann, P. and Davis, B.: “New Dispersive Mixers for Single Screw Extruders”, SPE ANTEC Tech. Papers, 277-284 (1998)
24. Danckwerts, P.V.: “Continuous Flow Systems”, Chem. Eng. Sci., **50**, 1-13 (1953), DOI: 10.1016/0009-2509(96)81810-0
25. Lidor, G., Tadmor, Z.: “Theoretical Analysis of Residence Time Distribution Functions in Plasticating Screw Extruders”, Poly. Eng. Sci., **16**, 450-462 (1976), DOI: 10.1002/pen.760160610
26. Danckwerts, P.V.: “The Definition and Measurement of Some Characteristics of Mixtures”, Appl. Sci. Res., **A3**, 279-296 (1952), DOI: 10.1007/BF03184936
27. Ottino, J.M.: The kinematics of mixing: stretching, chaos, and transport, Cambridge University Press, Cambridge (1989)
28. Ottino, J.M., Ranz, W.E. and Macosko, C.W.: “A Framework for Description of Mechanical Mixing of Fluids”, AIChE Journal, **27**, 565-577 (1981), DOI: 10.1002/aic.690270406
29. Avalosse, T. and Crochet, M.J.: “Finite-Element Simulation of Mixing: 2. Three-Dimensional Flow Through a Kenics Mixer”, AIChE Journal, **43**, 588-597 (1997), DOI: 10.1002/aic.690430304
30. Bolen, W.R., Colwell, R.E.: “Intensive Mixing”, Soc. Plast. Eng. J., **8**, 24 (1958)
31. Bird, R.B., Warner, H.R. and Evans, D.C.: “Kinetic Theory and Rheology of Dumbbell Suspensions with Brownian Motion”, Adv. Poly. Sci., **8**, 1-90 (1971), DOI: 10.1007/3-540-05483-9_9
32. Tadmor, Z.: “Forces in Dispersive Mixing”, Ind. Eng. Chem. Fundam., **15**, 346-348 (1976), DOI: 10.1021/i160060a022
33. Manas-Zloczower, I., Feke, D.L.: “Analysis of Agglomerate Separation in Linear Flow Fields”, Int. Polym. Process., **2**, 185-190 (1988), DOI: 10.3139/217.880185
34. Manas-Zloczower, I., Feke, D.L., “Analysis of Agglomerate Rupture in Linear Flow Fields”, Int. Polym. Process., **4**, 3-8 (1989), DOI: 10.3139/217.890003
35. Cheng, J.J., Manas-Zloczower, I.: “Flow Field Characterization in a Banbury Mixer”, Int. Polym. Process., **5**, 178-183 (1990), DOI: 10.3139/217.900178
36. Yao, W. G., Tanifuji, S., Takahashi, K. and Koyama, K.: “Mixing Efficiency in a Pin Section for Single-Screw Extruders”, Polym. Eng. Sci., **41**, 908-917 (2001), DOI: 10.1002/pen.10790
37. Bird, R. B., Stewart, W. E. and Lightfood, E. N.: Transport phenomena, 2nd Ed., Wiley & Sons, Inc., New Jersey (2002)
38. Carreau, P. J., PH.D. Thesis, University of Wisconsin – Madison, USA (1968)
39. Yasuda, K., Armstrong, R. C. and Cohen, R. E.: “Shear Flow Properties of Concentrated Solutions of Linear and Star Branched Polystyrenes”, Rheol. Acta, **20**, 163-178 (1981), DOI: 10.1007/BF01513059
40. POLYFLOW User Manual 18.1, chapter 21, 485-504, Canonsburg, USA (2017)
41. Fortin, M.: “Old and New Elements for Incompressible Flow”, Int. J. Num. Methods Fluids, **1**, 347-364 (1981), DOI: 10.1002/fld.1650010406

42. Michaeli, W.: Extrusion Dies for Plastics and Rubber, 2nd Ed., Hanser Publishers, Munich (1992)
43. Mohr, W. D., Saxton, R. L. and Jepson, C. H.: “Mixing in Laminar Flow Systems”, Ind. Eng. Chem., **49**, 1855-1856 (1957), DOI: 10.1021/ie50575a030